Journal of
Materials Chemistry A

ROYAL SOCIETY
OF CHEMISTRY

REVIEW

View Article Online
View Journal | View Issue

Cite this: *J. Mater. Chem. A*, 2020, **8**, 7569

Electrochemical deposition of metal–organic framework films and their applications

Xuan Zhang,[ab] Kai Wan,[b] Palaniappan Subramanian,[b] Maowen Xu,[a] Jiangshui Luo*[cd] and Jan Fransaer*[b]

Received 10th January 2020
Accepted 30th March 2020

DOI: 10.1039/d0ta00406e

rsc.li/materials-a

Metal–organic framework (MOF) thin films have received increasing attention for many applications, such as chemical sensors and membranes. Several techniques have been developed for the deposition of MOF films. In particular, the processing of electrochemical deposition of MOFs has only recently been initiated but stands out from other methods due to the mild preparation conditions, monitoring of continuous processes, precisely controllable synthesis parameters and potential for large-scale production. Recently, interest in the electrochemical deposition of MOF films has started to expand from their preparation to applications. In this review, we summarize and critically assess the state of the mechanism, the influence of parameters on electrochemical deposition of MOFs and their corresponding applications in different areas. Moreover, the strengths and shortcomings of different electrochemical deposition methods and their suitable scopes are discussed. Finally, the urgent challenges and future opportunities of electrochemical deposition of MOFs are highlighted.

1. Introduction

As new kinds of porous materials with high surface area, Metal–Organic Frameworks (MOFs), comprising coupling units (metal ions or metal-oxo clusters) coordinated by organic ligands, have received a lot of attention since being first defined in the 1990s by Yaghi and Li.[1] Their diverse structures and tunable properties (including pore size, metal center, functional linkers and post-synthetic modification) exhibit broad potential for different applications.[2–8] Efforts during the past two decades mostly focused on three aspects: establishment of new synthesis methods, construction of new MOF structures and

---

[a] *Key Laboratory of Luminescent and Real-Time Analytical Chemistry (Southwest University), Ministry of Education, School of Materials and Energy, Southwest University, Chongqing 400715, PR China. E-mail: xumaowen@swu.edu.cn*

[b] *Department of Materials Engineering, KU Leuven, Leuven 3001, Belgium. E-mail: jan.fransaer@kuleuven.be*

[c] *College of Materials Science and Engineering, Sichuan University, 610065, Chengdu, China*

[d] *Laboratory for Soft Matter and Biophysics, Department of Physics and Astronomy, KU Leuven, Leuven, 3001, Belgium. E-mail: jiangshui.luo@kuleuven.be*

Dr Zhang received his doctorate from the Department of Materials Engineering at KU Leuven in 2018. After completing his PhD, he worked as a postdoctoral fellow at the same institute. He obtained his BSc and MSc degrees in Physical Chemistry from Lanzhou University in China. He has published over 25 peer-reviewed journal papers. His current research focuses on electrodeposition of MOFs and carbon–metal composite electrode materials for sensors, separation, catalysis and energy storage and conversion devices.

Kai Wan is currently a PhD student in Materials Science at KU Leuven, Belgium. He received his B.S. in Chemistry from Huanggang Normal University in 2013. He then obtained his M.S. in Physical Chemistry from South China University of Technology in 2016. His research interests focus on functional materials for electrocatalysis and fuel cells.

exploration of their applications. These three aspects complement each other. Progress in the synthesis will not only offer more possibilities to obtain a variety of interesting structures but will also facilitate a broader range of MOF-related applications. Some of the applications are generally based on MOFs as powder (*e.g.* gas storage and drug delivery). But MOFs are preferably required in the form of surface layers/films for many other applications such as sensors, catalysis, electronic devices (including optoelectronic and electrochemical energy storage and conversion devices) and membranes.[9–11] Because of the demand for MOF films, several techniques have been developed in the past few years, including seeded growth or secondary growth,[12] Langmuir–Blodgett layer-by-layer deposition or liquid phase epitaxy,[13,14] dip coating,[15] evaporation induced crystallization,[16] spin coating,[17] gel-layer synthesis,[18] chemical vapor deposition[19] and other similar methods. However, these methods often involve multi-step and complex processing procedures or high-cost techniques, leading to low reproducibility, and they are often time- and resource-consuming. Moreover, some of these methods can only be used to prepare a few types of MOFs.

Compared with the above methods, electrochemical methods are considered as some of the most promising methods to prepare MOF films inspired by the first patent proposed by BASF.[20] On the one hand, electrochemical synthesis allows the large-scale production of MOFs in powder form, while on the other, it is also an effective method to synthesize thin films and coatings. Some of the salient features of the electrochemical deposition method are (i) there is no pre-treatment required except for simple cleaning of the substrate, (ii) the possibility to operate under milder conditions with short synthesis time, (iii) the possibility to monitor the process in real time and continuously which is useful for industrial scale operations, and (iv) the self-closing ability of electrochemical

Dr Palaniappan Subramanian has been a Postdoctoral Research Associate at KU Leuven in the Department of Materials Science and Engineering since February 2018. Design and development of nanomaterials for energy storage, conversion and bio-sensing applications, elucidating structure–property relationships using in situ spectroscopy and scanning electrochemical microscopy are some of his areas of research interest. He is a contributing author of more than 50 publications and 2 book chapters. He has co-authored 1 US patent filed on the development of metal oxide electrocatalysts for water splitting.

Dr Jiangshui Luo has been appointed by KU Leuven as a visiting professor (2019.02–2020.10). From 2008 to 2011, he participated in the establishment of a modern fuel cell lab at the NEXT ENERGY|EWE Research Center for Energy Technology in Germany. He completed his PhD study at KU Leuven within 2 years in November 2012. During his FWO Postdoctoral Fellow mandate at KU Leuven, he proposed and demonstrated protic organic ionic plastic crystals (POIPCs) as a novel type of proton conductor. His research interests include electrolytes, electrocatalysts, hydrogen bonding, barocaloric materials and scientometrics.

Prof. Maowen Xu is the leader of the Institute for Clean Energy & Advanced Materials of Southwest University. He earned his PhD degree from Lanzhou University in 2008. He worked as a postdoctoral scholar in Prof. John B. Goodenough's group at the University of Texas at Austin from 2010 to 2013. He has published over 180 peer-reviewed journal papers. His current research is focused on the design and synthesis of electrode materials for sodium ion batteries, lithium/sodium–sulfur batteries and solid state batteries.

Prof. Jan Fransaer is a full professor in the Department of Materials Engineering at KU Leuven, head of Surface and Interface Engineered Materials and a fellow of "The Electrochemical Society". He obtained his Masters in metallurgy at UGent and his PhD in materials engineering at KU Leuven. He was a postdoctoral fellow at Harvard, where he studied nucleation and phase transformations. He has published 230 research articles in peer-reviewed journals and filed 14 patents, related to his research, of which four have been licenced to industry. His scientific activities focus on electrodeposition and electrochemical processing, energy storage, computational fluid dynamics and colloidal physics.

deposition ensures high throwing power and fewer cracks in the film. More importantly, the parameters during electrochemical deposition can be easily and precisely controlled. Combined with the designable characteristics of MOFs, the highly controllable electrochemical deposition procedure is a promising strategy for tailor-making MOF films for desired applications. The salient features and advantages outlined above have evoked interest in electrodeposited MOF films for different applications in recent years as shown in Fig. 1.

Although some reviews related to the electrochemical synthesis of MOFs have been published, they are mostly focused on the synthesis and only a few targeted applications and related discussions are reviewed.[21,22] In the last few years, progress was made not only in the electrochemical deposition of MOFs, but also in various device fabrications using electrodeposited MOF films. The research on electrochemical deposition of MOFs has started to move from synthesis towards applications (see Table 1). For different applications, the requirements and challenges for MOF films are not the same. Therefore, this review focuses on three aspects: (1) the latest progress in the mechanism and the influence of parameters on MOF films associated with three types of electrochemical deposition of MOFs, (2) key developments in the applications of electrochemically deposited MOF films, and (3) the strengths and shortcomings of these three types of electrochemical deposition methods for different applications.

2. Electrochemical deposition techniques

The electrochemical deposition of MOFs can be classified into three types: anodic electrodeposition (AED), cathodic electrodeposition (CED) and electrophoretic deposition (EPD). The two former methods involve the *in situ* synthesis of MOFs on the substrate while EPD is a technique to deposit presynthesized MOFs. In this section, we will introduce the mechanism of electrochemical fabrication of MOFs and discuss the impact of key parameters on the electrochemical fabrication of MOF films.

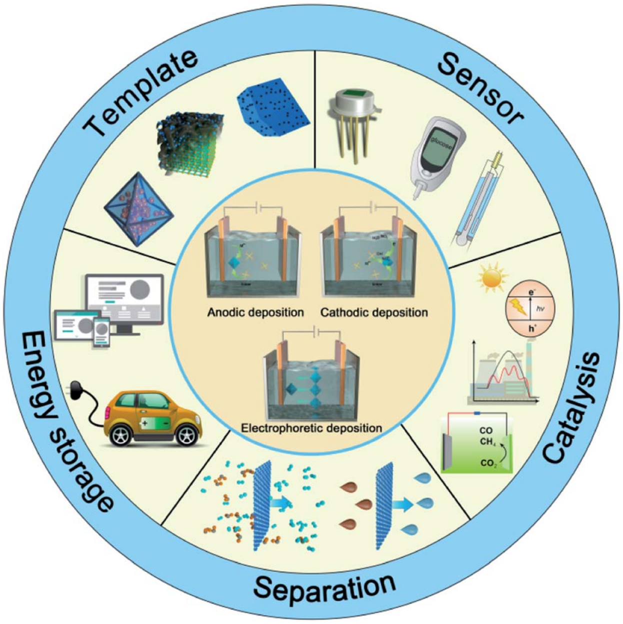

Fig. 1 Schematic diagram of the major applications of electrochemically synthesized MOF films.

2.1 Anodic electrodeposition

After the publication of the first patent by BASF, AED of MOFs has drawn the attention of researchers due to the milder and controllable conditions, time saving and the possibility of industry-scale production of MOF powders.[23–30] By anodically dissolving the metal substrate in a linker containing electrolyte, MOF formation occurs in the solution near the electrode surface, which can be processed in batch mode or in a continuous flow cell. Starting from this work, researchers at KU Leuven developed a method for the anodic electrodeposition of MOFs on a metal substrate. By carefully controlling the electrosynthesis conditions, such as current density, deposition time, and electrolyte composition, a compact film could be deposited on a metal substrate. In 2009, researchers at KU Leuven first proposed the patterned growth of Cu_3(benzene-1,3,5-tricarboxylate)$_2$($C_{18}H_6O_{12}Cu_3$, Cu-BTC) on a copper substrate.[31] By applying an anodic potential, copper is oxidized to Cu^{2+} electrochemically in a water–ethanol solution containing 1,3,5-benzenetricarboxylic acid (H_3BTC) and methyltributylammoniummethyl sulfate (MTBS) as a conductive salt. In this way, a densely packed film of Cu-BTC forms on a copper substrate within minutes.

The crystal size and thickness of the MOF films could be varied with the applied voltage (related to the concentration of metal ions near the surface). Also, a higher concentration of water in the synthesis mixture led to larger MOF crystals. In subsequent work, the AED conditions were studied for this archetypal MOF (Cu-BTC).[32–40] The charge required to oxidize the anode can be supplied in both amperometric (constant current) and potentiometric (constant voltage) modes. According to nucleation theory, higher current densities lead to smaller particle size. As the reaction proceeds, the average crystal size and thickness increase with increasing deposition time. In the end, the films are one to a few crystals thick. During prolonged growth, however, MOF films detach from the substrate, due to the anodic dissolution of the underlying substrate. The organic electrolyte often has low conductivity with a low energetic efficiency, which can be improved by increasing the temperature or through the addition of conductive salts. MTBS is the most common conductive salt for the electrochemical deposition of MOFs. Tetrabutylammonium tetrafluoroborate (TBATFB),[27,29] $LiClO_4$ (ref. 41) and $NaNO_3$ (ref. 42) were also used as conductive salt in some cases. It is worth mentioning that these conductive salts can get trapped in the pores of MOFs, leading to a decrease of the accessible surface area. Interestingly, it was found that TBATFB is not trapped inside the pores during anodic electrodeposition in spite of its large size.[29] In some studies, other kinds of additives (for

Table 1 Summary of electrochemical deposition of MOF thin films and their various applications

Sample	Method	Application
Cu-BTC	AED	Synthesis[32,34,36,38,40,44,47–50]
Cu-BTC	AED	Sensor[31,33,35]
Cu-BTC	AED	Catalysis[57]
Cu-BTC	AED	Separation[37,102]
Cu-BTC	AED	Template[39,117]
Cu-BTC	CED	Sensor[84,87–89]
Cu-BTC	EPD	Synthesis[67,72,91]
Cu-BTC	EPD	Sensor[92]
Cu-BDC, Cu-BTEC	AED	Synthesis[91]
Cu-BTEC	CED	Supercapacitor[106]
Cu(CHDA)	AED	Synthesis[44]
Cu(INA)$_2$	AED	Synthesis[44,50]
Cu-TDPAT/CCQDs	CED	Sensor[90]
Cu-TCA	AED	Sensor[78]
Co/Ni-BTC-DMF	AED	Template[116]
Co-BDC-DABCO	AED	Template[120]
Co-CA	CED	Template[62]
Ni-BTC, Fe-BTC, Fe/Ni-BTC	CED	Catalysis[96,97]
Ni-BDC-NH$_3$/CCQDs	CED	Sensor[89]
Zn-BTC, Eu-HBPTC	AED	Sensor[77]
Zn-BTC	EPD	Catalysis[68]
Mn/Mn-BTC	AED	Template[118]
Al-MIL-53, NU-1000	EPD	Synthesis[67]
Eu-TDC, Tb-BDC	CED	Sensor[64]
Eu-HBPTC, Tb-HBPTC, Gb-HBPTC	CED	Sensor[65]
Tb-BTC, Eu-BTC, Tb/Eu-BTC	EPD	Sensor[81]
UiO-66	AED	Synthesis[43]
UiO-66	EPD	Synthesis[67]
UiO-66/Ln, UiO-66-(COOH)$_2$, UiO-66-hybrid	EPD	Sensor[82]
UiO-66/C-QDs	EPD	Sensor[83]
Ir–Zn$_e$	AED	Sensor[76]
MIL-100	AED	Separation[53]
MIL-100	AED	Supercapacitor[105]
MOF-5	CED	Synthesis[55,56,58,59]
MOF-525	EPD	Catalysis[95]
NENU-3	AED	Sensor[35]
ZIF-4, ZIF-7, ZIF-8, ZIF-14, ZIF-67, ZIF-8	AED	Supercapacitor[107]
ZIF-67	AED	Template[119]
ZIF-8, ZIF-67, ZIF-71	CED	Synthesis[61]
ZIF-8	CED	Separation[103]
ZIF-7, ZIF-8	EPD	Separation[104]

example, modulators to control the crystal size and morphology) were added to the electrolyte, which affected the formation of intermediates or led to competition between the additives and the ligand towards the metal ions.[41,43] In the case of AED, the temperature exerts a significant influence on the solubility of linkers, conductivity of the electrolyte, kinetics of MOF formation and morphology of the resulting MOFs. Some of these factors (pH, deprotonation of linkers, hydration of metal ions, the solubility of linkers and conductivity of electrolyte…) can be tuned by varying the solvent composition.[31,34,36,38,44]

Bearing all this in mind, a comprehensive study of the mechanism of MOF crystal nucleation and growth during the anodic electrodeposition process was undertaken by researchers at KU Leuven.[45] As shown in Fig. 2A, the AED of MOF films consists of four phases:

(i) Initial nucleation: a critical concentration of metal ions forms upon anodic dissolution of a metal substrate. This stage can be clearly observed by detecting the mass change using EQCM. Once MOF crystals nucleate on the substrate, no new nucleation is needed for the deposition to proceed.

(ii) Growth of islands: the small MOF nuclei progressively grow into big crystals within minutes. In time, the size distribution and the average size of MOF crystals become broader and larger, respectively.

(iii) Intergrowth: there are two steps in this phase. The self-closing behavior of the electrochemical synthesis of MOF film can be understood in part by the different contributions of the applied potential (E):

$$E = E_0 + \eta_{\text{activation}} + \eta_{\text{ohmic}} + \eta_{\text{conc}}$$

where E_0 is the standard potential of anodic reaction, $\eta_{\text{activation}}$ is the activation overvoltage of metal dissolution, η_{ohmic} is the ohmic drop due to the resistance and η_{conc} is the concentration

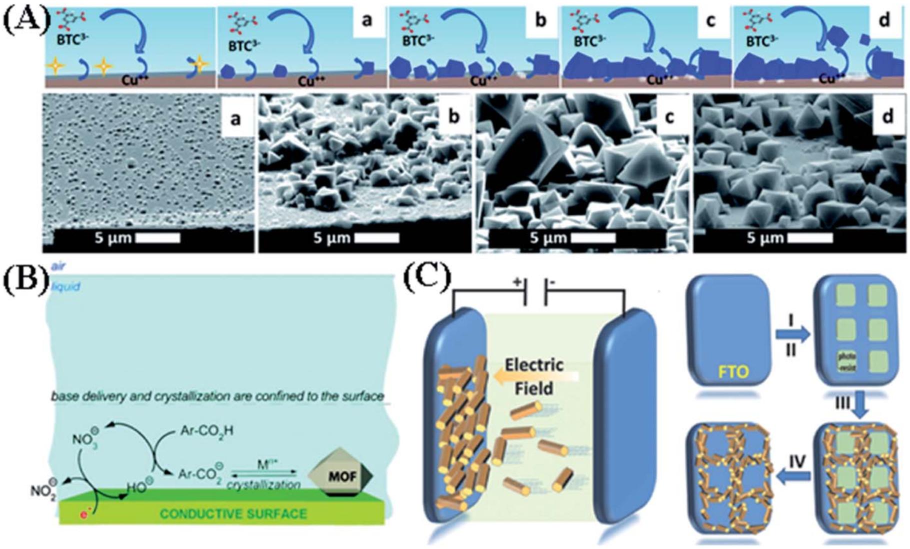

Fig. 2 (A) Proposed mechanism of anodic electrodeposition of MOFs and SEM pictures, taken at a 75° angle with the normal, of the four phases: (I) initial nucleation (a), (II) growth of islands (b), (III) intergrowth (c), and (IV) detachment (d). Copper-coated wafer substrate, 2 V *vs.* counter electrode, after 10 s, 10 min, 60 min and 125 min. Reproduced with permission from ref. 45. Copyright 2016, the Royal Society of Chemistry. (B) Mechanism of cathodic electrodeposition of crystalline MOFs. Cathodic electrodeposition of MOFs relies on the accumulation of OH^- ions. Reproduced with permission from ref. 55. Copyright 2011, American Chemical Society. (C) Schematic illustration of EPD of MOFs, showing the attraction of charged MOF particles toward an oppositely charged electrode using an applied electric field and illustration of the patterning of the MOF EPD film procedure: (I) spin coating a layer of photoresist on a bare FTO substrate, (II) using photolithography to create patterned squares of photoresist, (III) deposition of MOF particles on the conductive exposed FTO areas using EPD, and (IV) removal of the remaining photoresist squares to obtain the desired pattern. Reproduced with permission from ref. 67. Copyright 2014, Wiley-VCH.

overpotential. Before the substrate is fully covered by MOFs, MOFs will prefer to grow on the uncovered substrate due to a non-uniform current distribution, caused by an increase of η_{ohmic} and η_{conc} on those areas where a MOF layer is already present. After that, because of the small pore sizes and the large steric hindrance within MOFs, the linker molecules are too large to penetrate into the MOF structure. The MOF crystals grow at the MOF–solution interface rather than the MOF–substrate interface, which was proven using modified linkers (elemental marking with Cl or F) in a copper isonicotinate structure.[45]

(iv) Detachment: as the linkers cannot migrate through the MOF layer but copper ions can, the MOF layer grows at the MOF–solution interface. This implies that after a certain time, the copper underneath the MOF at the metal–MOF interface has dissolved so much that the MOF crystals detach from the substrate. Very recently, this four-step process was strongly supported by Dryfe *et al. via in situ* electrochemical atomic force microscopy.[46]

For the application of MOF films, the electrode structure and the mechanical properties of the MOF films are also critical. The most commonly reported MOFs show porosities restricted to the microporous regime (<2 nm), which makes the applications of MOF films suffer from diffusion limitations.[47] An important approach to reduce this diffusion limitation is the introduction of mesopores (2–50 nm) and macropores (>50 nm) into the MOF films that can shorten the diffusion paths and enlarge the effective surface area by enhanced mass and ion transport. Researchers at KU Leuven prepared a 3D hierarchical structure MOF coated electrode by combining a dealloying procedure with anodic electrodeposition.[48] A Ag–Cu alloy was used as an anode for preparing Cu-BTC. After application of a suitable voltage, the "noble" adatoms (*i.e.* Ag) are left behind and form a porous matrix structure during the dissolution of Cu, which forms MOFs inside the porous matrix. This 3D hierarchical structure MOF coated matrix electrode showed much higher surface area (7000 $m^2\ m^{-2}$) than the dealloyed structure without a linker (470 $m^2\ m^{-2}$) or pure copper plate derived MOF layers (2433 $m^2\ m^{-2}$). This 3D hierarchical structure not only increased the surface area of the electrode but also reduced the risk of detachment of the MOF film. In order to achieve a similar goal, Kuhn *et al.* used colloidal crystals of silica spheres as a template to prepare hierarchical macro-/microporous Cu-BTC composite electrodes.[49] Firstly, silica spheres were coated on a Au plate by a Langmuir–Blodgett (LB) technique. Thereafter, Cu was deposited on the surface of the silica sphere covered electrode by electrodeposition. After removal of silica spheres, an ordered macroporous Cu scaffold with open pores was obtained. Finally, dissolution of this porous Cu scaffold by electrochemical anodic oxidation in a linker-containing electrolyte created the desired MOF structure. In an attempt to further downsize MOF structures, Wouter *et al.* established a method to synthesize nanowires and three-dimensionally interconnected nanowire networks of Cu-MOFs, including both Cu(isonicotinate)$_2$[$C_{12}H_8O_4N_2Cu$, Cu(INA)$_2$] and Cu-BTC, by a combination of ion-track technology and electrochemistry.[50] They first prepared porous polycarbonate membranes *via* ion-track technology. Then metallic Cu was electrodeposited inside these porous polycarbonate membranes. In a last step, the metallic Cu nano-wires were anodically dissolved in a linker-containing solution, forming the desired MOFs with the structure of nanowires and nanowire networks. Similarly, using the two-step method ((I) deposition of metal and (II) anodic dissolution), MOFs can be anodically deposited on different kinds of substrates without the limitation of the corresponding metal substrates.[51,52]

The mechanical properties of MOF films can strongly affect their stability in device structures. Through nanoindentation and nanoscratch experiments, Tan and co-workers found that the particle size and the type of linker exert a large influence on the mechanical properties of Cu-based MOFs.[44] Among the three kinds of Cu-based MOFs {Cu(*trans*-cyclohexane-1,4-dicarboxylate)[$C_8H_{10}O_4Cu$, Cu(CHDA)], $Cu(INA)_2$ and Cu-BTC}, Cu(CHDA) exhibits the best mechanical performance with the highest stiffness (10.9 GPa) and hardness (0.46 GPa). In their more recent work, they modified the mechanical properties of Cu-BTC films by tuning the parameters of the anodic electrodeposition process. Not only does the reaction time (affecting the etching of the substrate) have an influence on the mechanical properties of the MOF film, the roughness of the substrate also affects the adhesion strength (the change of lift-off force).[32] Based on this, the group at KU Leuven compared the adhesion strength of different $Zr_6O_4(OH)_4$(1,4-benzenedicarboxylate)$_6$ ($C_{48}H_{28}O_{32}Zr_6$, UiO-66) films, prepared by anodic or cathodic electrodeposition.[43] Significantly enhanced adhesion strength of UiO-66 film could be achieved by anodic electrodeposition, caused by a metal oxide layer bridging the MOF layer and substrate.

In addition, anodic electrochemical synthesis offers additional degrees of freedom in the synthesis of MOFs, which allows it to be combined with other methods. The synergistic effect of two methods further facilitates the industrial production of MOFs and broadens the possibility of MOF film synthesis. A high-temperature high-pressure (HT-HP) electrochemical cell was used for combining the solvothermal method with anodic electrodeposition to prepare crystalline $Fe_3O(H_2O)_2OH$(benzene-1,3,5-tricarboxylate)$_2$ ($C_{18}H_8O_{16}Fe_3$, MIL-100) films,[53] which is hard to synthesize at low temperatures. The accessible synthesis temperature range can be enlarged by this method. Therefore, they used this cell to explore the temperature effect on the morphology of the well-studied Cu-BTC in their work as well. Cu-BTC crystals with an unusual cubic morphology deposited on the copper plate at 200 °C. Another benefit of this method is that the conductive salt, nitrates or acids can be avoided in the electrolyte due to the increase of conductivity and higher solubility of linkers. In addition, a new synergic strategy combining sonochemistry and electrodeposition for the synthesis of MOF powders was reported by Júnior *et al.*[54]

2.2 Cathodic electrodeposition

CED is based on the deprotonation of linkers through the electrochemical generation of hydroxide anions (metal ions are present in the electrolyte), facilitating the formation of MOF crystals on the substrate. This method was established by Li and Dincă. In their first study,[55] thin films of Zn_4O(1,4-benzodicarboxylate)$_3$($C_{24}H_{12}O_{13}Zn_4$, MOF-5) were deposited on FTO (cathode) by cathodic reduction of NO_3^- (Fig. 2B) as represented in eqn (1) and (2) at a constant potential of −1.6 V [*vs.* Ag/Ag(cryptand)$^+$] for 15 min in a deposition bath of DMF/water solution containing $Zn(NO_3)_2$, 1,4-benzenedicarboxylic acid (H_2BDC) and tetrabutylammonium hexafluorophosphate [$(NBu_4)PF_6$] as the metal source, linker and supporting electrolyte, respectively:

$$NO_3^- + H_2O + 2e^- \rightarrow NO_2^- + 2OH^- \quad (1)$$

$$H_2BDC + OH^- \rightarrow HBDC^+ + H_2O \quad (2)$$

In CED, the applied potential plays a critical role in the formation of MOF films. For example, metallic Zn deposits together with the MOF film, because the applied potential is sufficiently negative in this process. In their follow-up studies,[56] in order to avoid the electrodeposition of Zn, the reduction of triethylammonium (Et_3NH^+, see eqn (3)) which has a more positive reduction potential than the reduction of NO_3^- was chosen as an alternative to increase the local pH at the electrode surface. The product is trimethylamine and H_2. H_2 is a relatively inert molecule that has less influence on the formation of MOFs.

$$2R_3NH^+ \ (R = \text{alkyl}) + 2e^- \rightarrow 2R_3N + H_2 \quad (3)$$

$$R_3N + H_2O \rightleftharpoons R_3NH^+ + OH^- \quad (4)$$

Meanwhile, although the substrate has no relation to the metal source during CED, it still has a large influence on the reduction potential and the affinity between the MOF particles and the substrate, which is related to the formation and adhesion of MOF films.[56,57] Therefore, to minimize the overpotential for the reduction of Et_3NH^+, Pt was chosen as a working electrode. In a solution of Et_3NHCl and H_2BDC in DMF, the onset of proton reduction was at around −0.5 V [*vs.* Ag/Ag(cryptand)$^+$] with a peak current of −1.0 V [*vs.* Ag/Ag(cryptand)$^+$]. At this potential, no electrodeposition of Zn occurs. More interestingly, the MOF phase can be controlled by varying the concentration of Et_3NH^+ and the applied potential. At a concentration of 300 mM Et_3NH^+, the only phase that is formed is $(Et_3NH)_2Zn_3(BDC)_4$. When the concentration of Et_3NH^+ was reduced to 100 mM, exclusively $(Et_3NH)_2Zn_3(BDC)_4$ deposited at −1.10 V and a mixture of $(Et_3NH)_2Zn_3(BDC)_4$ and MOF-5 was obtained at −1.50 V. Based on this, either mixed films or sandwich-type bilayer surface structures could be deposited. Following these studies, Li and Dincă focused on studying the different CED parameters of MOF-5.[58] They found that Cl^- inhibits the formation of MOF-5. Also, water is not required initially, as it is generated during the process. In depositions conducted without nitrate-containing Zn^{2+} precursors, $Zn_2(BDC)(OH)_2$ would be formed. Based on these results, they proposed a possible transformation scheme shown in Fig. 3. Similar to the solvothermal method,[59] the MOF-5 formation is accelerated by nitrate, as it leads to the formation of an important

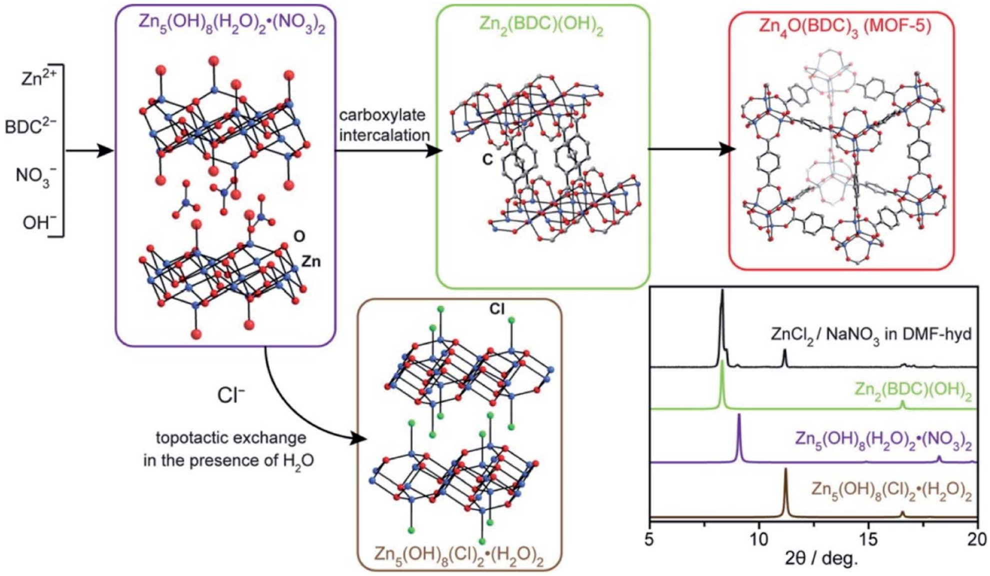

Fig. 3 Proposed transformation scheme to account for the different crystalline phases observed during the cathodic electrodeposition of MOF-5. The inset shows the experimental PXRD pattern of a sample deposited at −1.50 V on FTO in water-containing DMF (1.31 M H_2O) for 15 min with reagent concentrations of [$ZnCl_2$] = 150 mM, [$NaNO_3$] = 300 mM, and [H_2BDC] = 50 mM. The PXRD patterns of $Zn_5(OH)_8(H2O)_2\cdot(NO_3)_2$ and $Zn_5(OH)_8(Cl)_2\cdot(H_2O)_2$ were simulated. Reproduced with permission from ref. 58. Copyright 2015, American Chemical Society.

intermediate of layered $Zn_5(OH)_8(H_2O)_2\cdot(NO_3)_2$ phase. Therefore, NO_3^- not only facilitates the formation of a base for the deprotonation of the linker but also structurally forms the essential intermediate of layered $Zn_5(OH)_8(H_2O)_2\cdot(NO_3)_2$ phase during the CED process. Furthermore, they explored the influence of different oxygen sources, such as ClO_4^-, water and oxygen, on the formation of μ_4-O centers in MOF-5.[60] The relative crystallinity of these MOF films with other oxygen sources was lower than the crystallinity observed with nitrate, which is due to the role played by the layered zinc hydroxyl-nitrates as intermediates. Very recently, Guang *et al.* reported a comprehensive study of oxygen-assisted cathodic deposition of a series of ZIFs [including Zn(2-methylimidazole)$_2$($C_8H_{10}N_4Zn$, ZIF-8), Co(2-methylimidazole)$_2$($C_8H_{10}N_4Co$, ZIF-67) and Zn(4,5-dichloroimidazolate)$_2$($C_6H_2Cl_4N_4Zn$, ZIF-71] to avoid the plating of reduced metals.[61] The reaction arises from the reduction of O_2 to O_2^- on the electrode surface. Through the formation of the superoxide ion O_2^- or superoxo-Zn^{II} complex, the deprotonation of the linker will happen as shown in eqn (5):

$$2(Zn^{2+})(O_2^-) + 2[Zn(HmiM)_mL_n] \rightarrow 2[Zn(miM)(HmiM)_{m-1}L_n] + 2Zn^{2+} + H_2O_2 + O_2 \quad (5)$$

The deprotonated complex will subsequently evolve into a ZIF as proven by previous research on the hydrothermal synthesis.[62] Through this procedure, they deposited large-area uniform ZIF films of various thicknesses on different substrates without metallic zinc impurities. Additionally, the applied potential is not the only parameter influencing the CED of MOF films; deposition time, supporting electrolyte, substrate and additives also affect the MOF film formation. Yang *et al.* studied the influence of these parameters during the CED of terbium-succinate (TB-SA) from DMF containing ammonium nitrate onto transparent FTO electrodes.[63] Deposition time controls the thickness and mass loading of the MOF films. For the same deposition time, the thickness of the film can also be controlled by current density. But, when the current density was too large (>0.6 mA cm^{-2} in this case), the adhesion of the MOF films to the FTO was reduced. A similar situation was also observed in their later research on the CED of Eu(thiophene-2,5-dicarboxylate)($C_6H_2O_4SEu$, Eu-TDC).[64] Moreover, the higher current density will lead to more negative potentials during cathodic electrodeposition, which can lead to the formation of other impurity compounds on the substrate, for example reduction of metal ions. The conductivity and viscosity of an electrolyte depend in part on the concentration and/or nature of the supporting electrolyte and additives, which are key factors determining the current efficiency.[63,65] In addition, similar to the above discussion presented for the MOF-5 case, different supporting electrolytes and additives facilitate the formation of specific intermediates affecting the kinetics, and the nucleation and growth of MOFs.

2.3 Electrophoretic deposition

Another method for electrochemical deposition of MOF films is EPD. EPD is based on the transport of charged particles under the influence of an electric field, and the deposition of these particles at the oppositely charged electrode as schematically shown in Fig. 2C. Because of its low cost, and short formation time, EPD has been used in fabricating thin films for different fields, such as fabrication of wear-resistant and anti-oxidant ceramic coatings and preparation of functional films for advanced microelectronic devices.[66] Defects in MOFs (*e.g.* missing linkers and metal nodes) and the free functional groups in linkers (for example, the carboxylate group) could lead to surface charges on MOF particles. Compared with AED and CED, EPD is a two-step method, which includes an extra step for the synthesis of MOF particles. The first EPD of MOFs was done by Hupp *et al.*[67] Four kinds of MOFs {including Cu-BTC, Al(1,4-benzenedicarboxylate)($C_8H_5AlO_5$, Al-MIL-53), UiO-66 and $Zr_6(OH)_{16}$[1,3,6,8-tetrakis(benzoate)pyrene]$_2$($C_{88}H_{44}O_{32}$-Zr_6, NU-1000)} were successfully deposited by EPD at a constant DC voltage of 90 V onto fluorine doped tin oxide (FTO) (anode) from toluene suspensions of these MOFs. To show the versatility of the EPD of MOFs, two types of MOFs were patterned by photolithography on FTO step by step *via* EPD, creating a mixed structure of NU-1000/UiO-66 film. Among the parameters of EPD, the electrophoretic deposition time was explored for NU-1000. After 180 min of deposition, the surface of FTO is fully covered by NU-1000. In addition, the morphology of the MOFs also had an influence on the film formation process.[68] Han and his co-workers synthesized Zn_3(1,3,5-benzenetricarboxylate)$_2$($C_{18}H_6O_{12}Zn_3$, Zn-BTC) MOFs with different morphologies by controlling the mass fractions of $ZnCl_2$ during the solvothermal process. The rod-like Zn-MOFs form a smoother surface on the anode carbon paper in comparison with sheet-like and spherical ones. Unlike AED and CED, the key parameters for EPD, such as zeta potential, particle size distribution in the electrolyte, the conductivity of the suspension, *etc.*, have barely been investigated in the literature. Due to the synthesis conditions of pristine MOFs or the composition of the suspension solution, some MOF particles carry a positive charge.[69–71] Therefore, these MOF particles move to the cathode under the influence of an electric field. Once in contact with the cathode, the MOF crystals might be destroyed by reduction of the metal nodes inside the crystal structure during cathodic EPD.[72] In order to avoid this problem, Zhu *et al.* used hyaluronic acid as a charge reversal agent for Cu-BTC particles. The amount of hyaluronic acid had a large influence on the amount of deposited film. With enough additives, the Cu-BTC particles deposited on the anode without destruction of the MOF structure. All these results indicated that EPD of MOFs is a viable coating technique able to deposit various MOFs for a broad range of applications, especially for sensors and catalysis. We will discuss these in the following sections.

3. Applications

3.1 Sensors

Different kinds of sensors can be fabricated corresponding to different properties of MOFs, such as *e.g.* gas (liquid) absorption, luminescence (photoluminescence), and redox switching of the metal ion.[73,74] The tunable pore size and the specific chemical interactions of the internal surface and metal sites of MOFs provide opportunities to increase the selectivity and sensitivity of MOF based sensors. For most signal transduction schemes, thin MOF films need to be integrated into devices. On the other hand, thin film devices are easily stored, transported and recycled. Moreover, the good mass transport inside MOF films enables real-time detection of the analyte. The sensing mechanisms used for thin MOF film based sensors are gravimetric (Fig. 4A), optical (Fig. 4B) and electrochemical (Fig. 4C). The first sensor based on electrodeposited MOFs was proposed by researchers at KU Leuven in 2009.[31] In that article, they demonstrated the patterned growth of Cu-BTC on the electrode of a quartz crystal microbalance (QCMB) by anodic electrodeposition. The synthesis conditions were tuned to obtain a dense and smooth coating. This allowed the humidity of a flowing gas to be monitored *via* water adsorption onto the structure of Cu-BTC as shown in Fig. 4A. The sensor showed good reproducibility when cycled between dry and wet nitrogen flows.

Compared with other sensing mechanisms, changes of luminescence (including enhancement, shifting, or quenching) in MOFs have been the most widely used mechanism in MOF based sensors until now due to their wide range of applications (such as temperature, oxygen, pH, biomolecules and so on).[74,75] The first electrochemically synthesized, luminescent MOF thin film sensor was prepared by Mei-Lin Ho *et al.*[76] The Ir–Zn_e coordination compound was synthesized using $Ir(ppy)_2(H_2dcbpy)PF_6$(L-H_2, ppy = 2-phenylpyridine, H_2dcbpy = 4,4′-dicarboxy-2,2′-bipyridine) as a ligand and Zn as metal nodes. The Zn ions were produced by the anodic dissolution of Zn metal, predeposited on a stainless steel mesh. The influence of electrodeposition conditions such as voltage, time, and temperature on the MOF structures, particle size and photoluminescence properties, oxygen-sensing performance and other factors is explored in detail. Finally, MOFs synthesized at 5 V and 30 °C for 1 h exhibited the best performance with a deduced K_{SV} (associated Stern–Volmer quenching constant) value of 3.55, a detection limit of 0.050%, a recovery time of 21 s and a response time of 23 s toward oxygen. After 11 cycles of testing, >70% intensity could be maintained. Subsequently, a combination of glucose oxidase with this electrode could be used as a glucose sensor electrode exploiting the simultaneous depletion of oxygen with a concomitant increase of phosphorescence. The linear range for the determination of glucose was 0.1–6.0 mM with a limit of detection (LOD) of 0.05 mM and a response time of less than 120 s. Moreover, the biosensor showed similar results to isotope-dilution gas chromatography mass-spectrometry for detection of glucose in human serum. The fluorescent properties of Zn-based MOFs are also useful for the detection of nitro-explosives. Fluorescent Zn-MOF films were explored by Rong Cao and his co-workers.[77] The Zn_3(1,3,5-benzenetricarboxylate)$_2$($C_{18}H_6O_{12}Zn_3$, Zn-BTC) film was prepared *via* AED with two zinc plates as the anode and cathode in an aqueous solution (containing H_3BTC and NH_4F). 4-Nitrotoluene (4-NT), 2,3-dimethyl-2,3-dinitrobutane (DMNB), 2,4,6-trinitrotoluene (TNT), nitrobenzene (NB) and 1,3-dinitrobenzene (1,3-DNB) were chosen as target chemicals. TNT and 1,3-DNB (200 ppm) exhibited a significant quenching effect on the fluorescence of these MOF films with quenching percentages of 66% and 62%, respectively. The detection limits of these nitro explosives are as low as 0.5 ppm in solution. Compared with transition metal based MOFs, lanthanide MOFs attract more attention as luminescent sensors due to large Stokes shifts, intense sharp emissions, high color purity and a long lifetime.[74] These appealing luminescent properties of

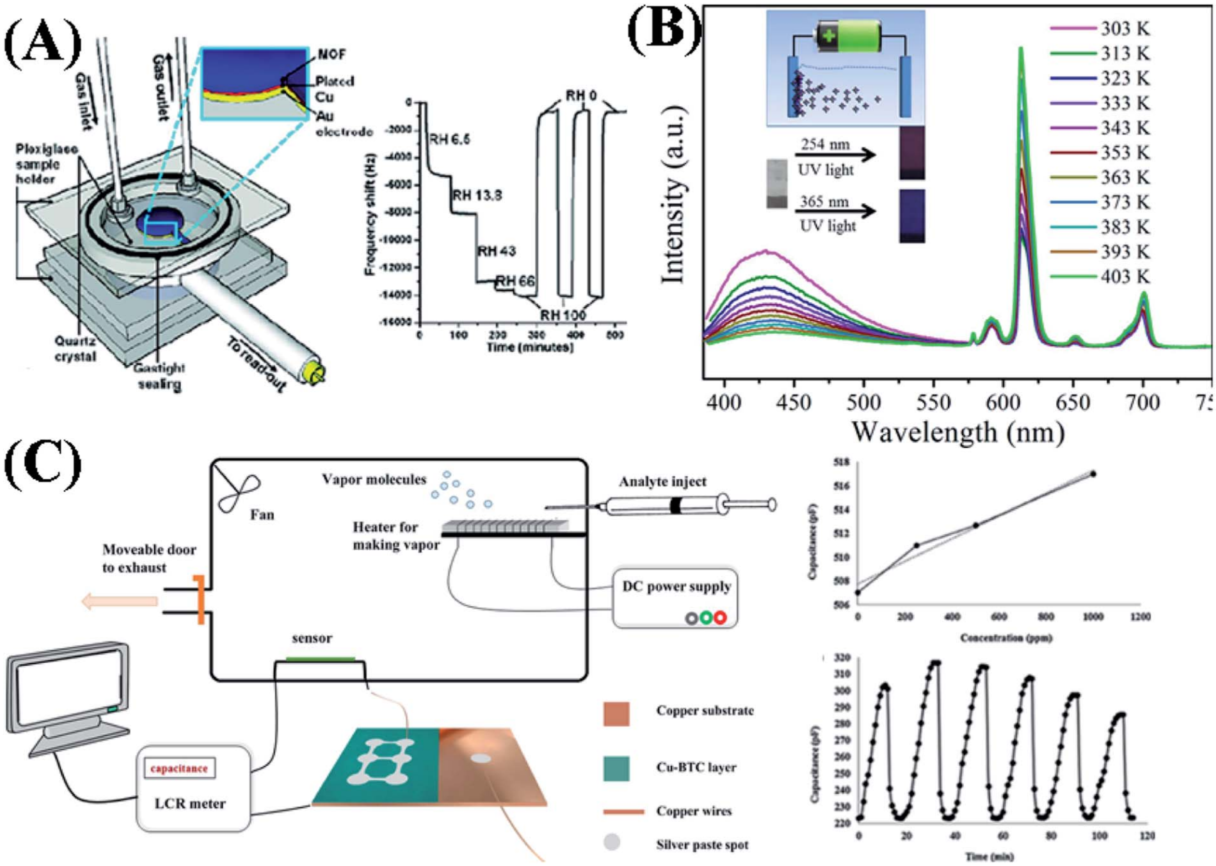

Fig. 4 (A) Electrochemically grown [$Cu_3(BTC)_2$] coatings in QCMB measurement of water adsorption. Schematic representation of the setup and signal upon adsorption of water from nitrogen streams at different RH values illustrating the reversibility and reproducibility. Reproduced with permission from ref. 31. Copyright 2009, Wiley-VCH. (B) Fabrication of composite films *via* the EPD method and emission spectra of the Eu@UiO-66-hybrid film recorded in the temperature range of 273–403 K with excitation at 330 nm. Reproduced with permission from ref. 82. Copyright 2018, American Chemical Society. (C) Schematic sensor setup used for VOC detection and fabricated capacitive nanosensor with Cu-BTC film and capacitance variation of sensor *vs.* methanol concentration (0–1000 ppm) upon applying 1 MHz, and LCR meter frequencies with the corresponding cycling behavior of the Cu-BTC-based capacitive sensor after introducing analytes with 500 ppm of methanol. Reproduced with permission from ref. 33. Copyright 2016, Elsevier.

lanthanide MOFs originate from f–f transitions with organic linkers acting as antennas. Interestingly, optical color changes of specific MOF films, when a change of applied potential happens, can be observed even by the naked eye. Lu *et al.* developed MOF-based electrochromic films with redox-active ligands [Cu_3(tricarboxytriphenyl amine)$_2$ ($C_{42}H_{24}O_{12}N_2Cu_3$, CuTCA)] on FTO (with pre-deposition of Cu particles on FTO) by anodic electrodeposition.[78] The fabricated film can achieve rapid switching speed (both coloration and bleaching time < 5 s), a high optical contrast of 65% @ 700 nm and long cycling ability (1000 cycles with <5% contrast attenuation). However, because of the high cost of these rare earth metals, AED is not suitable for preparing lanthanide MOFs. Yangyi Yang and his co-workers engineered a series of lanthanide MOF based sensors by cathodic electrodeposition. Their first work is related to carbonate detection.[65] A thin film of Eu(benzophenone-3,3′,4,4′-tetracarboxylate)(H_2O)$_2$ ($C_{17}H_{11}O_{11}Eu$, Eu-HBPTC) was coated on FTO by cathodic electrodeposition. Based on the same method, Tb-HBPTC and Gb-HBPTC were also synthesized successfully. The luminescent properties of Eu-HBPTC film for sensing carbonate in aqueous solution were then studied. When this film was immersed in 10^{-3} M CO_3^{2-} for two hours, the emission at 617 nm almost disappeared. The quenching effect can still be observed even in the presence of 10^{-6} M CO_3^{2-}. Common interferents such as Cl^-, ClO_4^-, BrO_3^-, IO_3^-, SO_4^{2-}, HPO_4^{2-} and PO_4^{3-} anions were tested under the same conditions. No significant change was observed for the fluorescence intensity, indicating the high selectivity of this carbonate sensor. In their follow-up work, Eu based MOF films with different linkers [thiophene-2,5-dicarboxylate (TDC) and naphthalene-2,6-dicarboxylate (NDC)] were studied for the sensing of nitroaromatic explosives[64] and picric acid,[79] respectively. Another lanthanide element used for luminescent sensors is Tb. Yangyi Yang *et al.* used different Tb based MOF films for the detection of Cu^{2+}.[63] A flower-shaped thin sheet comprising clusters of Tb-succinate MOFs was prepared by CED on FTO. Under optimal electrodeposition conditions (current density, time, supporting electrolyte, the addition of NaOH), a dense and smooth layer was obtained. The stability of this thin film in water and DMF was explored by immersing it into a solution for 3 days. There was no obvious decline in DMF, and more than 75% emission intensity ($^5D_4 \rightarrow {}^7F_5$ emission at 545 nm) could be retained in water. After immersion of this film in 1×10^{-3} M Cu^{2+}, the emission intensity decreased more than 85% in 10 min. A linear relationship between the emission intensity and the concentration of Cu^{2+} could be observed in the range from 1×10^{-5} M to 1×10^{-3} M with a K_{SV} of 6298 M^{-1}. Compared to powder samples, thin film samples showed a faster response. For the sensing of Cu^{2+} by Tb-SA films, interfering cations (K^+, Ba^{2+}, Mg^{2+}, Cd^{2+}, Ca^{2+}, Co^{2+}, Ni^{2+}, Zn^{2+} and Fe^{3+}) showed no obvious influence on the detection of Cu^{2+}. Based on the luminescence lifetime results with and without the addition of Cu^{2+}, the behavior of the quenching process is found to be static quenching. In addition, the color change under 254 nm UV-light and the peak changes in XRD indicate that this quenching effect could be caused by ion-exchange of Cu^{2+} into the TB-succinate structure. Following the same strategy, smooth and adherent thin films of Tb(benzene-1,3,5-tricarboxylate)($C_9H_3O_6Tb$, Tb-BTC) were coated on FTO as well, which showed an even higher K_{SV} (1.7×10^4 M^{-1}) than that of TB-succinate.[80] These studies indicate that linkers and metal ions in MOF structures can be easily tuned by CED under suitable electrodeposition conditions.

EPD was also used to prepare thin films of lanthanide MOFs. Recently, Rong Cao and his co-workers developed a sensor made by EPD. Continuous and dense Ln-BTC MOF films [including Tb-BTC MOF, Eu(benzene-1,3,5-tricarboxylate)($C_9H_3O_6Eu$, Eu-BTC) MOF and $Tb_{0.55}Eu_{0.45}$-BTC MOF] were rapidly (within 5 min) and easily coated on different substrates such as Zn, ITO and FTO.[81] Firstly, MOFs were prepared by a solvothermal method using different sources of metal ions. Then, these MOFs were dispersed into a CH_2Cl_2 solution for EPD using different substrates, voltages and deposition times. A layer of lanthanide MOFs was deposited on the positive electrode due to the free carboxylate group of these MOFs (negative charge). The as-prepared Tb-BTC films were used for the detection of different analytes: (1) Cr^{3+} in aqueous solution, (2) NB in an ethanol solution and (3) NB and TNT in the gas phase. All analytes showed clear luminescence quenching for the Tb-BTC films. Because of the separation of the synthesis and coating steps in EPD, predesigned and functionalized MOFs prepared by other methods can be deposited. The flexibility in choosing the desired MOF offered by the EPD method allows for further improvement in the sensing performance of MOF films. For example, Cao *et al.* reported a procedure to prepare lanthanide loaded UiO-66-$(COOH)_2$ film with hybrid linkers by EPD for temperature sensing.[82] They used post-synthetic exchange (PSE) and post-synthetic modification (PSM) to introduce a luminescent ligand (1,4-naphthalene dicarboxylic acid) and luminescent metal ions (Eu or Tb) into the UiO-66 structure, respectively. Moreover, the particle size and Ln content of Ln@UiO-66-hybrid MOFs can be easily controlled during the solvothermal process for the pristine UiO-66-$(COOH)_2$ MOF and PSM step. The resultant Ln@UiO-66-hybrid MOFs exhibited a blue emission from H_2NDC and a green emission from Tb^{3+} or red emission from Eu^{3+} (Fig. 4B). Under optimal conditions (type of metal precursor, Ln content and particle size), Eu@UiO-66-hybrid MOF film showed the best temperature-sensing ability with a relative sensitivity of 4.26% K^{-1}, between 303 K and 403 K. Carbon quantum dots (C-QDs) can also be doped into the UiO-66-$(COOH)_2$ structure to prepare C-QDs@UiO-66-$(COOH)_2$ film based on the same EPD procedure.[83] This film can be used to detect temperature changes in a lower temperature range (97–297 K) in comparison to the Eu@UiO-66-hybrid MOF with a relative sensitivity of 1.3% K^{-1}. In order to explore the possibility of AED of lanthanide MOF films without using costly lanthanide metal plates, a two-step method was proposed recently.[51] In the first step, a ZnO–Tb mixture was deposited on the surface of the substrate (Zn or Al). Then a layer of Tb-BTC was deposited on the substrate *via* a typical anodic electrodeposition of MOFs using a constant current in a water–absolute ethanol electrolyte containing H_3BTC and MTBS. The resulting Tb-BTC film showed the same morphology and luminescence properties as Tb-BTC films derived from a Tb plate. This Tb-BTC film has been successfully tested for the detection of 2,4-dinitrotoluene (DNT) by the quenching of luminescence effect. Surface-enhanced Raman scattering (SERS) of noble metal nanoparticles can be used to detect the "fingerprint" signature of an analyte. In order to prevent the noble metal nanoparticles from aggregating, MOFs can be used as good carriers for loading these particles due to their high surface area and porosity. However, the balance between maintaining the structure of the MOF and the increasing number of Raman "hot spots" at the junctions of these nanoparticles is the bottleneck. In order to solve this problem, Haitao and his co-workers constructed core–shell Cu-BTC@Ag nanoparticles on a screen-printed carbon electrode with a controllable structure by a two-step CED,[84] *i.e.* CED of Cu-BTC on a screen-printed carbon electrode with subsequent CED of Ag nanoparticles. After CED, the structure of the Cu-BTC can be maintained well. The resulting samples showed high SERS activity for detecting 4-aminothiophenol (LOD of 0.5 nM) and a series of polycyclic aromatic hydrocarbons (LOD from 0.15 nM to 20 nM for different molecules) with high stability and reproducibility.

Electrochemical sensors are the largest and the most versatile group of chemical sensors and are widely used in daily life. These sensors use conductometric, capacitive, and amperometric detection methods and impedance analysis.[85] M. H. Sheikhi *et al.* fabricated a MOF based capacitive nanosensor by anodic electrodeposition of Cu-BTC.[33] A thin film (5 μm) of Cu-BTC was coated on a patterned Cu plate as exhibited in Fig. 4C. This sensor was used to detect ethanol and methanol vapors based on changes in capacitance caused by the absorption of volatile organic compounds (which changes the dielectric constant). The linear range of this sensor for ethanol and methanol is 0–1000 ppm with a LOD of 39.1 ppm and 130.0 ppm for methanol and ethanol, respectively. Recently, an amperometric-based sensor was prepared by Qu and his co-workers.[35] In their work, anodic electrodeposition was employed to prepare an electro-active metal–organic framework film (NENU-3), which is composed of Cu-BTC encapsulating phosphotungstic acid, on a copper plate. This electrode was used to detect bromate, which is correlated with certain health and environmental issues,[86] by the electrocatalytic reduction of bromate. Some kinetic parameters of the electrocatalytic reduction of bromate, such as the catalytic rate constant (k_s) and the electron transfer coefficient (α), were derived from CV and LSV data. At a potential of −0.3 V, a wide linear range (0.05–72.74 mM) with an LOD of 12 μM was achieved by this chronoamperometric method. Moreover, inorganic anti-interferents such as Na^+, K^+, Cl^-, NO_3^-, NO_2^-, SO_4^{2-}, ClO_3^-, NH_4^+ and CO_3^{2-} do not have an obvious influence on the signal of the electrocatalytic reduction of bromate. Except for bromate, Nianjun *et al.* studied the sensing performance of Cu-BTC films on glassy carbon electrodes (deposited by CED) for different kinds of organic molecules, including nicotinamide adenine dinucleotide, diethylstilbestrol, estradiol, hypoxanthine, tartrazine, sunset yellow, and xanthine.[87] They found that the applied cathodic potential has a clear influence on the morphology, thickness and sensing performance of the Cu-BTC films. The same method was used by Ji and his co-workers for electrochemical determination of bisphenol A as well.[88] The highest peak currents of Cu-BTC films for determination of bisphenol A were achieved at a potential of 0.496 V (*vs.* SCE). At this potential, the Cu-BTC films showed a large linear range (5.0 to 2000 nM) with a low LOD (0.72 nM). The results show that Cu-BTC films can reach a comparable analytical performance (for determination of bisphenol A) with high-performance liquid chromatography. Electrochemical sensors based on MOFs can be used for chiral recognition and resolution of organic molecules as well. Xuan Kuang *et al.* successfully co-deposited chiral carbon quantum dots (CCQDs) and MOFs [Ni(1,4-benzenedicarboxylate)-NH_3, $C_8H_4O_4Ni\text{-}NH_3$, and Ni-BDC-NH_3] on Cu foil by CED.[89] This electrode exhibited good selectivity and high sensitivity to penicillamine enantiomers with a good linear relationship between current density and L-PA% in the racemic mixture. In their following work,[90] the preparation of a CCQDs/[Cu_3(2,4,6-tris(dimethylamino)-1,3,5-triazine)(H_2O)$_3$]·$10H_2O\cdot 5DMA$ ($C_{27}H_{18}O_{15}N_6Cu_3$, Cu-TDPAT) composite electrode was performed following the same procedure. The composite electrode not only shows quantitative analysis towards tyrosine (Tyr) enantiomers but also presents the ability to determine L-Tyr% in racemic mixtures. The same detection method for H_2O_2 sensing was explored by Nianjun Yang *et al.*[91] In their paper, Cu-based MOFs with different organic ligands were deposited on a glassy carbon electrode by the CED method. Based on their theoretical and experimental results, not only the morphology but also the electrochemical behavior and active sites of the Cu-MOFs can be tuned by different organic ligands, including 1,3,5-benzenetricarboxylic acid, 1,4-benzenedicarboxylic acid, and 1,2,4,5-benzenetetracarboxylic acid. The Cu-MOF with 1,3,5-benzenetricarboxylic acid linkers exhibited the highest current response for H_2O_2 at a potential of −0.7 V (*vs.* SCE). This work also contains stability results after the electrochemical test, which is important for practical application of such sensors but is rarely reported. FT-IR, XPS, and XRD data and SEM images of these Cu-MOFs before and after measurements were recorded. After 10 min testing time, the structure of the Cu-MOFs was not changed, but decomposition and collapse of these MOFs were observed after long duration stability tests (*e.g.* 24 h). In order to improve the conductivity of MOF based electrodes for sensors, Jianshan *et al.* prepared Cu-BTC/multi-walled carbon nanotube (MWNT) multilayer films by a two-step EPD from two different solutions, including Cu-BTC and MWNTs, respectively.[92] The electrode with eight layers (four layers of Cu-BTC and four layers of MWNT films) showed the best performance for detecting glucose with a sensitivity of 3878 μA cm^{-2} mM^{-1}.

3.2 Catalysis

One of the earliest proposed applications for MOFs was catalysis.[93] Their large internal surface area, uniform pore size, abundant active sites and good thermal stability (up to 500 °C for some MOFs[94]) play important roles in catalysis.[3] Compared with powder catalysts, catalyst layers in the form of thin films on a solid carrier/support could be beneficial for recycling, stability and reduction of cost in heterogeneous catalysis. Moreover, the self-closing behavior of AED and CED enables the preparation of catalyst layers on a 3D structured substrate. For example, a thin layer of Cu-BTC was deposited on Ni foam (NF) *via* CED by Changwen Hu *et al.* (Fig. 5A).[57] This sample was used as a catalyst for photocatalytic hydrogen production. The photocatalytic hydrogen production rates of MOF-199 on the NF and powdered Cu-BTC are 8.0 mmol h^{-1} g^{-1} and 7.2 mmol h^{-1} g^{-1} with eosin-Y as the photosensitizer, respectively. When Pt is used as a co-catalyst, the photocatalytic hydrogen production rates of different samples increase to 24.4 mmol h^{-1} g^{-1} (film sample) and 22 mmol h^{-1} g^{-1} (powder sample). After 3 h, Cu-BTC/NF showed a 3 times higher hydrogen production rate than powdered Cu-BTC. Moreover, after use, Cu-BTC/NF can be easily recycled, which is attractive for industry scale processes.

In situ synthesis of catalyst layers is highly recommended for electrochemical or photoelectrochemical reactions not only because of the enhancement of reactivity and ease of recycling but also because it help in avoiding the use of binders. For electrochemical or photoelectrochemical reactions, the active materials must be coated on a conductive substrate using additional binders, such as Nafion and PTFE. These non-conductive additives increase the resistance, cause partial blocking of pores and active sites, hamper the transport of ions and increase the processing time and cost. More importantly, these issues increase with increasing aerial mass loading of the catalyst. To address these challenges, binder-free electrodes are highly desired. Electrochemical deposition is one of the most promising ways to solve/circumvent the above problems. Hod and co-workers proposed a strategy to immobilize an Fe-porphyrin catalyst into $Zr_6O_4(OH)_4$(4,4′,4″,4‴-(porphyrin-5,10,15,20-tetrayl) tetrabenzoate-H_2)$_3$($C_{144}H_{82}O_{32}Zr_6$, MOF-525) thin films for the electrochemical reduction of CO_2.[95] First, MOF-525 was coated on an FTO substrate by EPD. After a solvothermal post-metalation with iron chloride, the target electrode configuration could be accomplished with high areal concentrations equivalent to ~900 monolayers of surface-adsorbed Fe-TPP. At an overpotential of 650 mV for the reduction of CO_2 to CO in DMF electrolyte containing 1 M $TBAPF_6$, the main product is a mixture of CO and H_2 with a 100% faradaic efficiency (54 ± 2 and 45 ± 1% for CO and

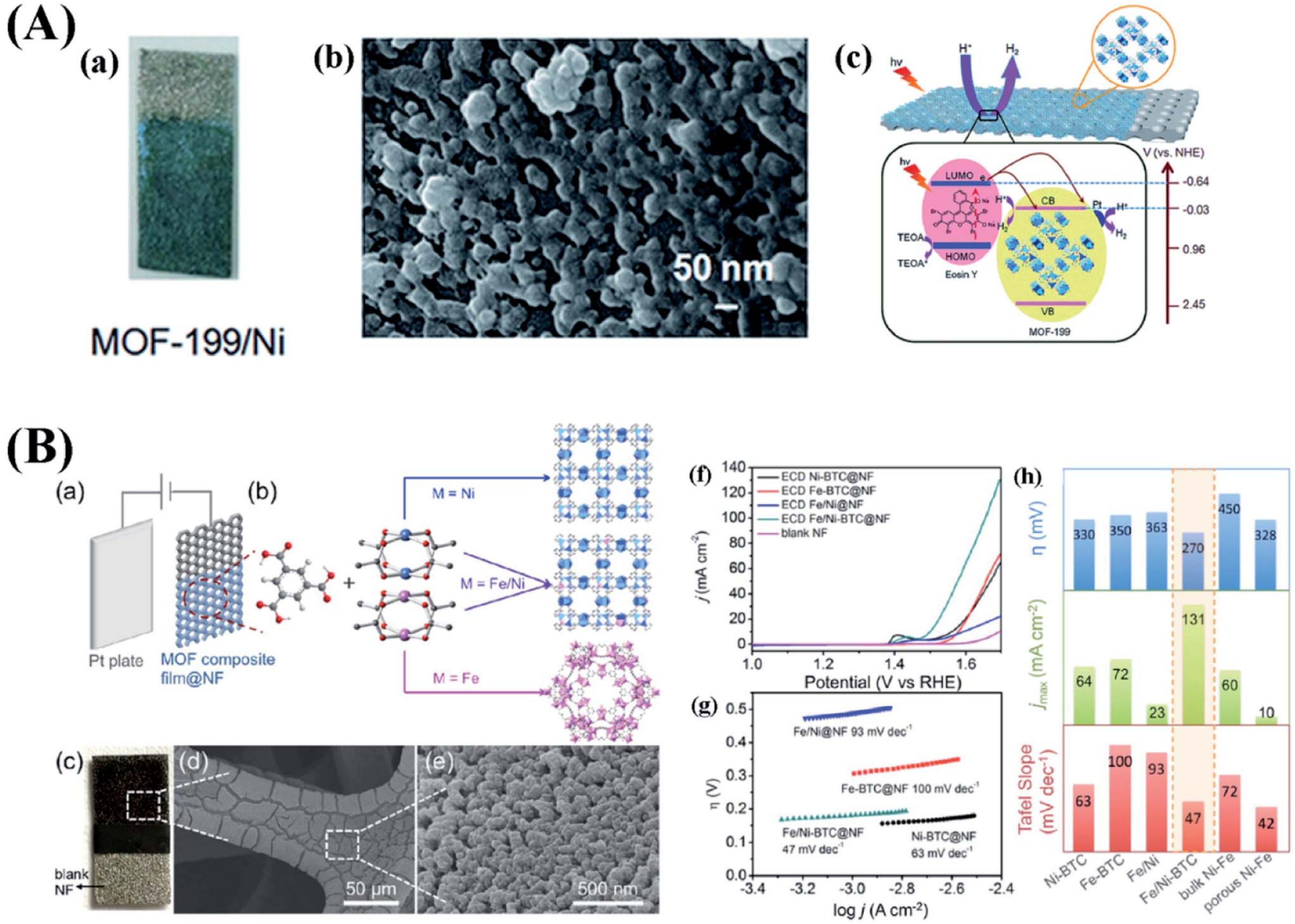

Fig. 5 (A) (a) Optical photograph and (b) SEM image of the MOF-199/Ni film prepared by electrodeposition with (c) the schematic of the eosin-Y sensitized photocatalytic process on the MOF-199/Ni film. Reproduced with permission from ref. 57. Copyright 2016, the Royal Society of Chemistry. (B) (a) ECD process of Fe/Ni-BTC MOF thin films. (b) Design and synthesis of Fe/Ni-BTC MOFs. (c) Optical image, (d) scanning electron microscopy (SEM) image, and (e) higher-magnification image of Fe/Ni-BTC@NF. (f) LSV curves of ECD Ni-BTC@NF, ECD Fe-BTC@NF, ECD Fe/Ni@NF, ECD Fe/Ni-BTC@NF, and NF measured at 2 mV s^{-1}. (g) Tafel plots of ECD Ni-BTC@NF, ECD Fe-BTC@NF, ECD Fe/Ni@NF, and ECD Fe/Ni-BTC recorded at 1 mV s^{-1}. (h) Comparison of ECD Ni-BTC, ECD Fe-BTC, ECD Fe/Ni, ECD Fe/Ni-BTC, bulk Ni–Fe oxides, and porous Ni–Fe oxides. Reproduced with permission from ref. 96. Copyright 2016, American Chemical Society.

H_2 formation, respectively). The current was limited by the rate of change of diffusion through the MOF structure. For future work, improvement of the rate of diffusion could be a key to realizing better catalysts. In the following year, a pure MOF catalyst for electrochemical reduction of CO_2 was reported by Kang *et al.*[68] A solvothermal method was used to synthesize Zn-BTC with different morphologies by changing the mass fraction of $ZnCl_2$ in the synthesis solution. These Zn-BTC MOFs with different morphologies were deposited onto carbon paper by EPD from a methanol/DFG solution, using a constant potential (10–50 V) for one hour. They found that not all the morphologies of Zn-BTC form smooth layers. When the mass fractions of $ZnCl_2$ were 0.44 and 0.5, the irregular surface is dominant. This is most likely caused by the particle size of the suspension and the uneven current distribution at the edges. Then these electrodes were used as a cathode in the electrochemical reduction of CO_2 with different ionic liquid electrolytes. Under the same conditions, the sheet-like Zn-BTC covered electrode showed the highest current density with the highest electrochemical surface area. Gas chromatography (GC) and ^{1}H-NMR identified CH_4 as the main reaction product with a selectivity of 80%. Such a high selectivity is rare. This study also explored in more detail the effect of different electrolytes and metal electrodes. A higher current density and higher selectivity of the sheet-like Zn-BTC covered electrode than other metal electrodes for the reduction of CO_2 were observed. Due to the strong interaction between fluorine and CO_2, $BmimBF_4$ was found to be the most effective electrolyte. Another example of a binder-free thin film MOF electrode for electrochemical reactions is related to the oxygen evolution reaction (OER), which is a critical half-reaction for electrochemical water splitting and in rechargeable metal–air batteries due to the sluggish kinetics of the OER. In order to avoid binder issues, CED was used by Bo Wang *et al.* for preparing Ni_3(benzene-1,3,5-tricarboxylate)$_2$($C_{18}H_6O_{12}Ni_3$, Ni-BTC) MOF layers.[96] To further improve the catalytic ability of Ni-BTC, 10% (based on the molar ratio of two metal sources) of iron ions were introduced into the electrolyte. At a potential of −1.5 V *vs.* Ag/AgCl with a deposition time of 30 s, Ni-BTC, MIL-100 and Fe/

Ni-BTC MOF thin films were coated on NF as shown in Fig. 5B. The NF-Fe/Ni-BTC MOF shows the best OER performance with an overpotential of only 270 mV at 10 mA cm^{-2} and with the lowest Tafel slope (47 mV dec^{-1}). At 1.5 V *vs.* RHE, the current density of NF-Fe/Ni-BTC thin films was around 100 times higher than that of Fe/Ni-BTC powder (prepared by a solvothermal method) coated on glassy carbon electrodes. The NF-Fe/Ni-BTC electrode also showed no signs of degradation at 1.53 V *vs.* RHE during 15 h. As mentioned in Section 2.2, the applied potential has a large influence on the formation of MOF films during CED. Chen and his co-workers reported that a metallic Fe nanostructure was formed when CED of Fe-BTC was performed at −1.5 V (*vs.* SCE).[97] They prepared different Fe-BTC films at different negative potentials (−1.1 V, −1.5 V and −1.9 V). The Fe/Fe-BTC film deposited at −1.5 V exhibited the loosest morphology and best electrochemical catalytic performance for H_2O_2 reduction, because of more electrochemically active sites originating from the loosest morphology of the Fe/Fe-BTC film deposited at −1.5 V.

3.3 Separation

Gas and molecular separation have proven to be very promising in addressing the energy and environmental challenges. MOF films or membranes are promising candidates to achieve this goal. MOF films for gas and molecular separation have been studied during the last decade.[6,98–101] Compared to other methods, patterned growth of MOFs is one of the advantages of electrochemical deposition which benefits the fabrication of microseparators. Van Assche *et al.* presented an AED method to prepare a microchannel separator device by patterning PEEK covered copper sheets as precursor substrates with subsequent anodic electrodeposition of Cu-BTC on the exposed copper surface as shown in Fig. 6A.[37] The microseparator was subsequently used to separate a mixture of methanol and *n*-hexane vapors in breakthrough experiments. The microseparator exhibited a lower pressure drop and faster adsorption rate than a conventional packed bed. Moreover, the microseparator can be used for testing the separation and adsorption properties of microporous films on supports, which is difficult in conventional devices. Based on the same approach, MIL-100 was explored as a microseparator material for the separation of methanol and *n*-hexane mixtures (Fig. 6B).[53] A thin layer of MIL-100 was pattern-deposited by a high-temperature anodic electrodeposition process on the surface of a microseparator. Using a N_2 flow, a mixture of *n*-hexane and methanol vapors was delivered to the microseparator. The breakthrough of methanol

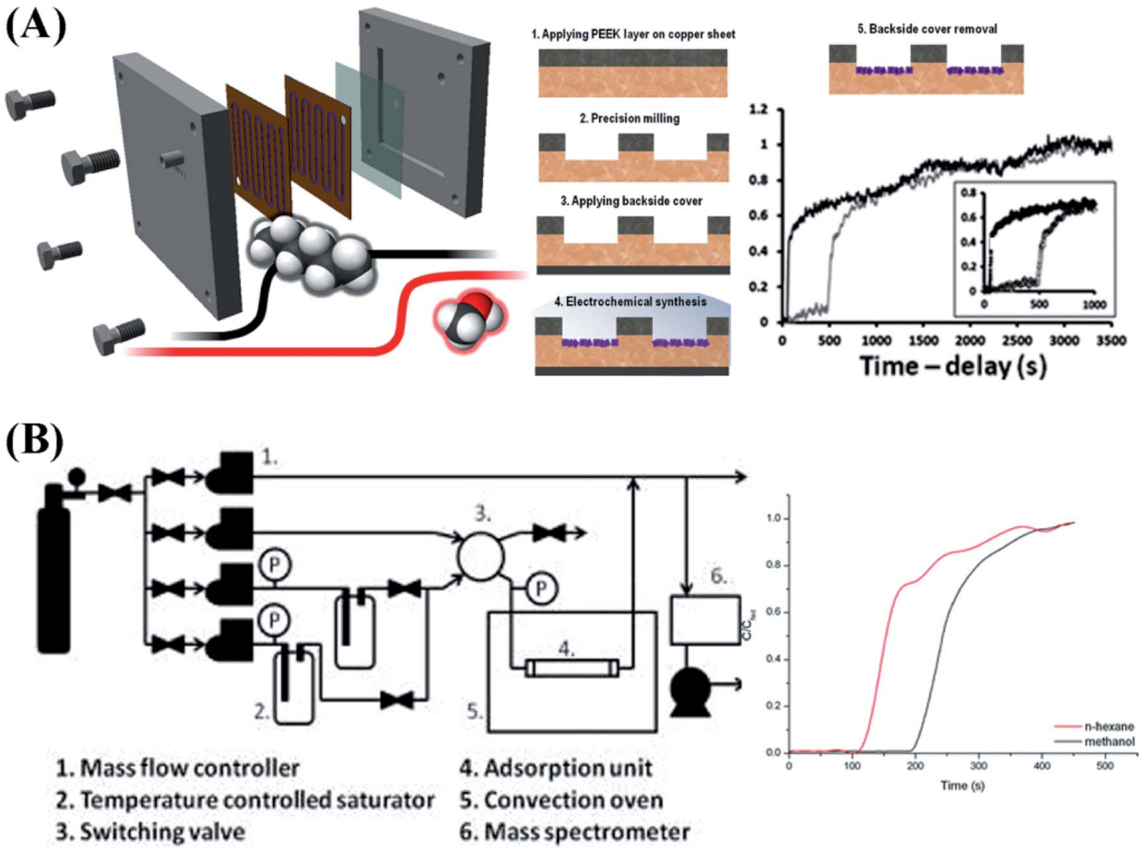

Fig. 6 (A) Overview of the fabrication steps for a MOF coated microseparator and the corresponding binary breakthrough profiles of a MOF coated microseparator with *n*-hexane (10.21% in feed stream) and methanol (2.11% in feed stream) vapor. Reproduced with permission from ref. 37. Copyright 2013, Elsevier. (B) Overview of the setup for a MOF coated microseparator and breakthrough curves of a MIL-100(Fe) microfluidic device fed by a 40/60 methanol–*n*-hexane blend in nitrogen carrier gas. Reproduced with permission from ref. 53. Copyright 2013, the Royal Society of Chemistry.

occurred 80 s later than *n*-hexane after passing through this MIL-100 based microseparator. Recently, electrodeposition of metal–organic framework film on porous substrates for separation applications was developed by several groups. The research groups from KU Leuven realized a uniform *in situ* growth of a Cu-BTC selective layer on a poly(ether sulfone) (PES) polymer substrate by AED.[102] Because of the solid interface of the electrode and controllable AED procedure, this method can overcome the main problem of conventional interfacial polymerization caused by two different immiscible solvents and the uncontrollable issue of counter-diffusion. The resulting Cu-BTC/PES films showed 99.7% rejection of Rose Bengal. In addition, Lai *et al.* fabricated ZIF-8 type MOF membranes on an anodic aluminum oxide (AAO) substrate by CED.[103] With increasing deposition time, the thickness of the ZIF-8 layer can be tailored ranging from 50 nm to 500 nm. The thickest films exhibited superior performance for gas separation of C_3H_6/C_3H_8 with 182 GPU (1 GPU = 3.35×10^{-10} mol m^{-2} s^{-1} Pa^{-1}) C_3H_6 permeance and 142 selectivity at room temperature. During the EPD procedure, the unavoidable holes (larger than the size of MOF particles) are impermissible in separation related applications. A two-step approach (including seeding by CED and an intergrowth step) was developed by Agrawal *et al.*[104] Both defect-free ZIF-8 and ZIF-7 films were successfully deposited on AAO. The ZIF-8 membrane exhibited a high H_2 permeance of 8.3×10^{-6} mol m^{-2} s^{-1} Pa^{-1} and good gas selectivities of 7.3, 15.5, 16.2, and 2655 for H_2/CO_2, H_2/N_2, H_2/CH_4, and H_2/C_3H_8, respectively.

3.4 Energy storage

The large surface area and presence of transition metal sites make MOFs attractive for energy storage and conversion devices, such as Li-ion batteries, metal–air batteries, fuel cells, supercapacitors…. The poor electrical conductivity of most MOFs is the greatest impediment to using MOFs in these applications. The first report in this research area utilizing electrodeposited MOFs was published in 2014. In this paper, a high-temperature anodic electrodeposition process was used to prepare MIL-100 powder in less than one hour, much faster than hydrothermal methods.[105] However, due to the low electronic conductivity of this MOF, the MOF powder was scraped from the synthesis electrode, and then mixed with carbon nanotubes and carbon black to fabricate a supercapacitor electrode. The effect of the hydrated ion size of the electrolyte on the electrochemical behavior of this MIL-100 (Fe)-MOF was explored. Unfortunately, the reductive dissolution and low conductivity of the MOF hamper the capacitance and lifetime of this supercapacitor. Similarly, Naseri *et al.* first synthesized Cu_2(1,2,4,5-benzenetetracarboxylate)($C_{10}H_2O_8Cu_2$, Cu-BTEC) on a graphite electrode by cathodic electrodeposition.[106] Afterwards, poly-*ortho*-aminophenol (POAP)/(Cu-BTEC) composite films were prepared by the electropolymerization of POAP from a Cu-BTEC suspension. Through the combination of Cu-BTEC with POAP, the capacitance (241 F g^{-1}) is around 1.5 times higher (241 F g^{-1}) than that of a pure POAP electrode. After 1000 charge/discharge cycles, the capacitance of the POAP/Cu-BTEC electrode retained 91% of its initial value. The first pure MOF film electrode for energy storage was synthesized by Worrall *et al.*[107] In this work, a series of ZIFs [Zn(imidazole)$_2$($C_6H_6N_4Zn$, ZIF-4), Zn(benzimidazole)$_2$($C_{14}H_{10}N_4Zn$, ZIF-7), ZIF-8, Zn(2-ethylimidazole)$_2$($C_{10}H_{16}N_4Zn$, ZIF-14) and ZIF-67] were coated on Zn or Co electrodes *via* anodic electrodeposition with careful control of the reaction conditions. The resulting ZIF-67 coated Co electrodes exhibited an areal capacitance of 10.45 mF cm^{-2} at a scan rate of 0.01 V s^{-1}, which is seven times higher than the previous highest reported value for "additive-free" MOFs. This value is even higher than values reported for MOF/graphene composite materials.

3.5 Template synthesis of nanostructured materials

MOFs are considered as ideal self-sacrificing templates and precursors for preparing various carbon and metal-based nanomaterials due to their high surface area and tunability of the structures. The resulting materials are widely used in the fields of sensors, catalysis and energy storage and conversion devices. Because of the remarkable device performances, the number of publications based on such "MOF-derived materials" has seen an explosive growth during the last five years.[107–115] Since MOFs are not directly used in these applications, we put all cases related to MOFs as templates and precursors in this section. In order to replicate the porous structure of MOFs, Worrall *et al.* electrodeposited a layer of Cu-BTC on copper foil by anodic electrodeposition.[39] The resulting MOF film was subsequently used for the electrodeposition of Au. Part of the resulting Au nanostructure shows structural features of the Cu-BTC template up to dimensions < 2 nm. This film proved to function as a surface enhanced Raman spectroscopy substrate able to detect 4-fluorothiophenol. Besides, *in situ* growth of MOF films on substrates can avoid the addition of polymer binders and additives, which are commonly used to fix MOF-derived materials on a substrate. These additives increase the "dead weight" of the materials, increase the resistance, reduce the utilization of the electrode materials and impede mass transport. 2D-layered Ni–Co mixed MOFs [Ni(benzene-1,3,5-tricarboxylate)(DMF)$_2$($C_{15}H_{17}O_8N_2Ni$,Ni-BTC-DMF)] were deposited directly on nickel foam by anodic electrodeposition (Fig. 7A) as supercapacitor electrodes. After pyrolysis and activation, a mesoporous, layered Ni–Co mixed metal oxide–carbon composite electrode was obtained without any binder and without additional processing steps.[116] This electrode exhibits an excellent rate performance of 93% at current densities from 1 to 20 mA cm^{-2} with a capacitance of 2098 mF cm^{-2} (1 mA cm^{-2}), low resistance and excellent cycling stability, in spite of high mass loading (13 mg cm^{-2}).[116] This method was also extended to synthesize glucose sensors. With the same procedure, hierarchical Cu@porous carbon electrodes were fabricated by the *in situ* growth and subsequent pyrolysis of Cu-BTC (Fig. 7B).[117] The resulting electrode shows a high sensitivity (10.1 mA cm^{-2} mM^{-1}), and could be a promising candidate for non-invasive glucose monitoring. In the same fashion, Linnemann *et al.* synthesized Mn_3O_4/C film on stainless steel by thermolysis of Mn/Mn_3(benzene-1,3,5-tricarboxylate)$_2$($C_{18}H_6O_{12}Mn_3$, Mn-BTC) bilayered films as shown in Fig. 7C

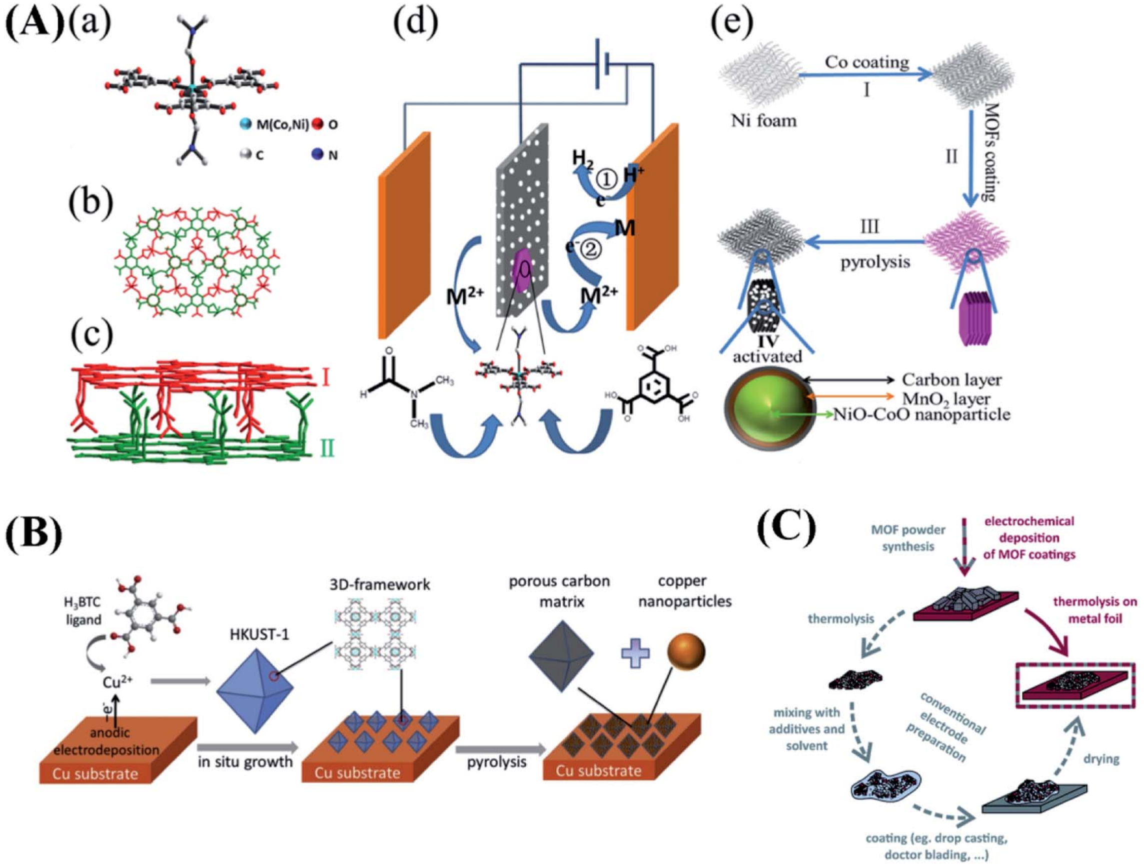

Fig. 7 (A) (a) Perspective views of the crystal structure showing the coordinative environment around the metal center in M(HBTC)(DMF)$_2$ (all H atoms are omitted for clarity); (b) packing of three 2D layers of M(HBTC)(DMF)$_2$ to generate a supramolecular framework by short contact stacking from the *c* axis (different layers are denoted in different colors); (c) view of the structure from the *b* axis; (d) schematic representation of anodic electrodeposition of MOFs; (e) schematic illustration of the process to prepare 2D-CMO material on NF. Reproduced with permission from ref. 116. Copyright 2017, Elsevier. (B) Schematic illustration of the synthesis of a Cu@porous carbon matrix on a copper foam substrate. Reproduced with permission from ref. 117. Copyright 2018, Elsevier. (C) Preparation of MOF-derived carbon composite electrodes by either thermolysis of electrochemically deposited MOF films in one step (red) or thermolysis of MOF powder and conventional electrode preparation in several steps (grey). Reproduced with permission from ref. 118. Copyright 2017, the Royal Society of Chemistry.

(prepared by anodic electrodeposition).[118] According to the voltammetric features, the integral capacitance of the bilayered system can be divided into three parts, including 160 F g^{-1} referring to Mn, 116 F g $^{-1}$ referring to Mn$_3$O$_4$ and 102 F g^{-1} referring to MnO$_2$, respectively. Compared with this strategy, conventional MOF-derived electrode preparations are both time and resource consuming. Moreover, the decrease of the effective electrochemical area and the increase of resistance caused by the binder can be avoided. Very recently, this route was also used for the electrocatalytic oxygen evolution by Wei and co-workers.[62] Firstly, a layer of Co(II)(H$_2$-CA)$_2$(H$_2$O)$_2$ (H$_3$CA = cyanuric acid) nanofibers was deposited on nickel foam by CED using the reduction of nitrate for the deprotonation of the linker at a potential of −1.2 V (*vs.* Hg/HgO). After pyrolysis at 300 °C for 2 h in air, this MOF converts to Co$_3$O$_4$ nanoparticle decorated carbon–nitrogen nanosheets. Then, this metal oxide and carbon composite binder-free electrode was used for the OER in 1 M KOH. A current density of 25 mA cm^{-2} was obtained at an overpotential of only 245 mV. Meanwhile, this electrode showed no degradation during a 20 h test at an overpotential of 370 mV. The same strategy for self-supported Li-ion battery anodes, based on ZIF-67 derived Co$_3$O$_4$, was reported by Kening *et al.*[119] In this work, metallic Co was deposited on the surface of vertically standing Ti nanowires and subsequently subjected to anodic dissolution in a solution with a linker to form a ZIF-67 layer. After pyrolysis, the self-supported Co$_3$O$_4$ polyhedra/Ti nanowire electrode exhibited a capacity of 700 mA h g^{-1} at a specific current density of 1.0 A g^{-1} with good stability (maintaining 2000 charge/discharge cycles without decay) for Li ion battery anodes. Except for energy storage devices and sensors, binder-free electrodes also benefit electrochemical catalysis. Qin *et al.* fabricated hollow, polyhedral structures, composed of Co$_3$O$_4$ nanocrystals and carbon quantum dots imbedded in a nitrogen-doped amorphous carbon matrix, grown on a Co foil electrode by anodic co-electrodeposition of Co$_2$(1,4-BDC)$_2$(DABCO)·4DMF·H$_2$O {DABCO = (1,4-diazabicyclo[2.2.2]octane)} and carbon quantum dots.[120] The resulting electrodes (pyrolyzed at 300 °C in air) displayed good electrochemical activity for oxygen evolution with an overpotential of 301 mV at a current density of 100 mA cm^{-2}. The Tafel slope of this electrode is 115 mV dec^{-1}, substantially lower than that of the electrode without carbon quantum dots (184 mV dec^{-1}). It can be seen that the co-deposition of MOFs with other materials is one effective way to further improve the performance of electrodes based on the electrochemical deposition of MOFs. In addition, similar structures can also be achieved by cathodic electrodeposition of MOFs.[62] In this work, Co(II)$(H_2CA)_2(H_2O)_2$ (H_3CA = cyanuric acid) was electrodeposited directly on Ni foam at room temperature by deprotonation of a linker based on electrochemical generation of hydroxide anions (reduction of NO_3^-). After pyrolysis at 300 °C in air, this electrode showed an overpotential of 390 mV to drive a catalytic current density of 100 mA cm^{-2} for oxygen evolution.

4. Summary and perspectives

MOFs are attractive materials for both scientists and engineers as evident from the large number of research papers published in the last two decades.[121–124] Devising a new MOF structure, studying the properties of new MOFs and tuning the structure of MOF units are more easily studied using MOF powders. However, the performances of MOF derived devices mostly depend on the properties of MOF films. To fulfill the requirements of commercial devices based on MOF materials, the interest in deposition methods for MOF films is growing. Compared with other methods, electrodeposition enjoys unparalleled advantages for the synthesis of dense and continuous MOF films, as well as high versatility, convenience and inexpensiveness of the electrodeposition technique. Electrodeposition is capable of device-quality and designable deposition due to the time monitoring and rapid signal feedback of electrodeposition. In this review, we summarized the recent progress of electrodeposition methods for MOF films and their promising applications. Three electrodeposition methods, AED, CED and EPD, are discussed (focusing on both the electrodeposition mechanisms and the impact of key parameters on electrodeposition). Five main applications of electrodeposited MOF films have been addressed, including sensing, catalysis, separation, energy storage, and template synthesis of nanostructured materials. Although the fabrication and application of electrodeposited MOF films have made great progress, there are still a few key challenges in this field, which also provide future research opportunities. As shown in Table 2, because of different mechanisms underlying AED, CED and EPD, different electrochemical deposition methods show different pros and cons. These pros and cons and how these characteristics affect the applications are discussed below:

(1) AED: because of the high current density attainable, high adaptability and high purity of the resulting MOF films based on anodic electrodeposition, AED exhibited promising potential for use in modern industrial processes. Anodically electrosynthesized MOF films are more compact than films derived from the other two electrochemical methods. The films also display on average higher adhesion strengths, which is perhaps caused by the formation of an oxide layer between the substrate and the MOF films serving as a bridging layer. This bridging layer can prevent detachment during subsequent processing steps or tests (*e.g.* pyrolysis). Therefore, anodic electrodeposition could be a better approach than the other two electrochemical methods for *in situ* growth of MOF-derived materials on the substrate. In addition, if the MOF film based devices are operated under harsh conditions (*e.g.* strong agitation, gas evolution, …), strong adhesion strength is necessary. It should be noticed that the enhanced adhesion strengths have a prerequisite relationship with the detachment of MOF crystals caused by anodic corrosion of the substrate. This is a balance between anodic corrosion of the substrate and formation of MOFs. Currently, there are no better methods except for optimizing the experimental conditions to find the balance point. Using a metallic electrode as the source of metal cations (instead of metal salts), the formation of corrosive ions or by-products can be avoided. However, the correspondence between the metallic electrode and the resulting MOF node is the main limitation of AED.

(2) CED: similarly, a dense and continuous MOF film can be prepared by CED as well. Unlike AED, any conductive substrate can be used as an electrode for CED of MOF films. Furthermore, the incorporation of a second (or more) metal node into the framework can be easily achieved by CED if the formation of these multi-metallic MOFs should be thermodynamically and kinetically feasible. In the case of CED, the potential plays a critical role in the resulting MOF films. Compared with AED, there are more competition reactions on the cathode. In most cases, the impurity of the metallic structure (originating from cathodic deposition of metals) is hard to avoid especially for the metal ions with more positive reduction potential. Moreover, the structures of the resulting MOF films are sensitive to reduction potential as well.

(3) EPD: theoretically speaking, any kinds of MOFs can be deposited on a substrate by EPD. If a specific or complex MOF structure is useful for the desired applications, EPD could be a better choice. In contrast to AED and CED, EPD is a coating technique rather than a synthesis method. An additional synthesis step is necessary for EPD of MOFs. Therefore, the advantages inherent to the electro-synthesis of MOFs such as

Table 2 Pros and cons of three electrodeposition methods for deposition of MOF films

	Applicability	Purity	Continuity and compactness	Adhesion strengths	Limitation of the substrate
AED	Medium	High	High	High	Limited
CED	Low	Medium	High	Medium	No limit (conductive)
EPD	High	High	Low	Low	No limit (conductive)

milder synthesis conditions and shorter synthesis time are not present in the EPD of MOF films. On the other hand, the separation of synthesis and deposition steps means that the MOFs can be functionalized in advance. Voids and cracks are hard to avoid in EPD, which will be the Achilles' heel for some applications (*e.g.* separations). When the continuous and dense film is not necessary (*e.g.* catalysis), EPD could be used for coating MOF film easily and efficiently. However, the mechanical fragility issues of MOF films prepared by EPD should be carefully considered.

From a broader point of view, at the early stage of research, most studies focus on some archetypal MOFs, such as Cu-BTC and MOF-5, which are notoriously simple to prepare. Recently, based on the better understanding of the principles of electrodeposited MOFs, such as critical concentration during AED and the formation of an essential intermediate during CED, more and more different kinds of MOFs are deposited by electrodeposition as shown in Table 1. However, due to the large number of members in the MOF family (more than 70 000), it is necessary and urgent to know the commonalities and differences behind the electrodeposition processes of these MOFs, for instance, how the deposition parameters (such as linkers, nodes, additives, pH…) affect the formation of MOF layers (the nucleation and crystal growth). Meanwhile, even though controllable thickness and crystal size have been achieved by electrodeposition, optimization of microstructures, such as research on defects, grain boundaries and channel orientations, is rare. In addition, with the development of MOF research, new types of MOFs have exhibited promising performance for desired applications, such as conductive MOFs, multi-metallic MOFs (consisting of multiple metal nodes within a single crystal) and multivariate metal–organic frameworks (consisting of multiple linkers of different functionalities within a single crystal). Electrodeposition could be a promising method to prepare these new types of MOF films. Last but not least, the stability of MOF films (both mechanical and chemical) is always a challenge before taking technology from laboratory to applications. Therefore, we recommend an analysis of stability for all reported studies.

Nowadays, studies of MOF films are shifting from synthesis towards their applications. The versatility of electrochemical deposition is a powerful asset in the preparation of MOF films for different applications. We sincerely hope that this review will facilitate the discovery and understanding of electrochemical deposition of MOF films and inspire more researchers to join this area.

Conflicts of interest

There are no conflicts to declare.

Acknowledgements

X. Zhang is grateful for PDM funding (18/149) from KU Leuven Internal Funds. X. Zhang and J. Fransaer are grateful for the FWO project (12ZV320N). K. Wan is grateful for the Overseas Study Program of Guangzhou Elite Project. M. W. Xu appreciates support from the National Natural Science Foundation of China (No. 21773188). J. Luo acknowledges the Research Foundation – Flanders (FWO) for a Research Project (G0B3218N) and a Research Grant (1529816N). Funding from the National Natural Science Foundation of China (No. 21776120) is acknowledged. This project has received funding from KU Leuven (C16/17/005 and IDO/12/006).

References

1 O. M. Yaghi, G. Li and H. Li, *Nature*, 1995, **378**, 703–706.
2 H. Furukawa, K. E. Cordova, M. O'Keeffe and O. M. Yaghi, *Science*, 2013, **341**, 1230444.
3 J. Lee, O. K. Farha, J. Roberts, K. A. Scheidt, S. T. Nguyen and J. T. Hupp, *Chem. Soc. Rev.*, 2009, **38**, 1450–1459.
4 S.-L. Li and Q. Xu, *Energy Environ. Sci.*, 2013, **6**, 1656–1683.
5 A. Morozan and F. Jaouen, *Energy Environ. Sci.*, 2012, **5**, 9269–9290.
6 S. Qiu, M. Xue and G. Zhu, *Chem. Soc. Rev.*, 2014, **43**, 6116–6140.
7 J. Ren, H. W. Langmi, B. C. North and M. Mathe, *Int. J. Energy Res.*, 2015, **39**, 607–620.
8 C. G. Silva, A. Corma and H. García, *J. Mater. Chem.*, 2010, **20**, 3141–3156.
9 A. Betard and R. A. Fischer, *Chem. Rev.*, 2012, **112**, 1055–1083.
10 D. Bradshaw, A. Garai and J. Huo, *Chem. Soc. Rev.*, 2012, **41**, 2344–2381.
11 O. Shekhah, J. Liu, R. A. Fischer and C. Woll, *Chem. Soc. Rev.*, 2011, **40**, 1081–1106.
12 M. A. Snyder and M. Tsapatsis, *Angew. Chem., Int. Ed.*, 2007, **46**, 7560–7573.
13 O. Shekhah, H. Wang, M. Paradinas, C. Ocal, B. Schüpbach, A. Terfort, D. Zacher, R. A. Fischer and C. Wöll, *Nat. Mater.*, 2009, **8**, 481–484.
14 O. Shekhah, H. Wang, D. Zacher, R. A. Fischer and C. Wöll, *Angew. Chem., Int. Ed.*, 2009, **48**, 5038–5041.
15 X. L. Liu, Y. S. Li, G. Q. Zhu, Y. J. Ban, L. Y. Xu and W. S. Yang, *Angew. Chem., Int. Ed.*, 2011, **50**, 10636–10639.
16 R. Ameloot, E. Gobechiya, H. Uji i, J. A. Martens, J. Hofkens, L. Alaerts, B. F. Sels and D. E. De Vos, *Adv. Mater.*, 2010, **22**, 2685–2688.
17 S. Mintova and T. Bein, *Adv. Mater.*, 2001, **13**, 1880–1883.
18 A. Schoedel, C. Scherb and T. Bein, *Angew. Chem., Int. Ed.*, 2010, **49**, 7225–7228.
19 I. Stassen, M. Styles, G. Grenci, H. V. Gorp, W. Vanderlinden, S. D. Feyter, P. Falcaro, D. D. Vos, P. Vereecken and R. Ameloot, *Nat. Mater.*, 2016, **15**, 304–310.
20 U. Mueller, H. Puetter, M. Hesse and H. Wessel, *BASF Aktiengesellschaft*, 2007.
21 H. Al-Kutubi, J. Gascon, E. J. R. Sudhölter and L. Rassaei, *ChemElectroChem*, 2015, **2**, 462–474.
22 W.-J. Li, M. Tu, R. Cao and R. A. Fischer, *J. Mater. Chem. A*, 2016, **4**, 12356–12369.
23 M. Hartmann, S. Kunz, D. Himsl, O. Tangermann, S. Ernst and A. Wagener, *Langmuir*, 2008, **24**, 8634–8642.

24 W. W. Lestari, M. Adreane and H. Suwarno, *J. Math. Fundam. Sci.*, 2017, **49**, 213–224.

25 W. W. Lestari, M. Arvinawati, R. Martien and T. Kusumaningsih, *Mater. Chem. Phys.*, 2018, **204**, 141–146.

26 M. Maes, F. Vermoortele, L. Alaerts, J. F. Denayer and D. E. De Vos, *J. Phys. Chem. C*, 2010, **115**, 1051–1055.

27 S. Mandegarzad, J. B. Raoof, S. R. Hosseini and R. Ojani, *Appl. Surf. Sci.*, 2018, **436**, 451–459.

28 R. S. Kumar, S. S. Kumar and M. A. Kulandainathan, *Electrochem. Commun.*, 2012, **25**, 70–73.

29 R. S. Kumar, S. S. Kumar and M. A. Kulandainathan, *Microporous Mesoporous Mater.*, 2013, **168**, 57–64.

30 H.-m. Yang, X. Liu, X.-l. Song, T.-l. Yang, Z.-h. Liang and C.-m. Fan, *Trans. Nonferrous Met. Soc. China*, 2015, **25**, 3987–3994.

31 R. Ameloot, L. Stappers, J. Fransaer, L. Alaerts, B. F. Sels and D. E. De Vos, *Chem. Mater.*, 2009, **21**, 2580–2582.

32 I. Buchan, M. R. Ryder and J.-C. Tan, *Cryst. Growth Des.*, 2015, **15**, 1991–1999.

33 M. S. Hosseini, S. Zeinali and M. H. Sheikhi, *Sens. Actuators, B*, 2016, **230**, 9–16.

34 A. M. Joaristi, J. Juan-Alcañiz, P. Serra-Crespo, F. Kapteijn and J. Gascon, *Cryst. Growth Des.*, 2012, **12**, 3489–3498.

35 E. Shi, X. Zou, J. Liu, H. Lin, F. Zhang, S. Shi, F. Liu, G. Zhu and F. Qu, *Dalton Trans.*, 2016, **45**, 7728–7736.

36 T. R. C. Van Assche, N. Campagnol, T. Muselle, H. Terryn, J. Fransaer and J. F. M. Denayer, *Microporous Mesoporous Mater.*, 2016, **224**, 302–310.

37 T. R. C. Van Assche and J. F. M. Denayer, *Chem. Eng. Sci.*, 2013, **95**, 65–72.

38 T. R. C. Van Assche, G. Desmet, R. Ameloot, D. E. De Vos, H. Terryn and J. F. M. Denayer, *Microporous Mesoporous Mater.*, 2012, **158**, 209–213.

39 S. D. Worrall, M. A. Bissett, P. I. Hill, A. P. Rooney, S. J. Haigh, M. P. Attfield and R. A. W. Dryfe, *Electrochim. Acta*, 2016, **222**, 361–369.

40 P. Schafer, M. A. van der Veen and K. F. Domke, *Chem. Commun.*, 2016, **52**, 4722–4725.

41 S. Khazalpour, V. Safarifard, A. Morsali and D. Nematollahi, *RSC Adv.*, 2015, **5**, 36547–36551.

42 P. Mirahmadpour, D. Nematollahi, M. H. Banitaba and S. S. H. Davarani, *J. Inorg. Organomet. Polym. Mater.*, 2015, **26**, 376–383.

43 I. Stassen, M. Styles, T. Van Assche, N. Campagnol, J. Fransaer, J. Denayer, J.-C. Tan, P. Falcaro, D. De Vos and R. Ameloot, *Chem. Mater.*, 2015, **27**, 1801–1807.

44 B. Van de Voorde, R. Ameloot, I. Stassen, M. Everaert, D. De Vos and J.-C. Tan, *J. Mater. Chem. C*, 2013, **1**, 7716.

45 N. Campagnol, T. R. Van Assche, M. Li, L. Stappers, M. Dincă, J. F. Denayer, K. Binnemans, D. E. De Vos and J. Fransaer, *J. Mater. Chem. A*, 2016, **4**, 3914–3925.

46 S. D. Worrall, M. A. Bissett, M. P. Attfield and R. A. W. Dryfe, *CrystEngComm*, 2018, **20**, 4421–4427.

47 K. Shen, L. Zhang, X. Chen, L. Liu, D. Zhang, Y. Han, J. Chen, J. Long, R. Luque and Y. Li, *Science*, 2018, **359**, 206–210.

48 N. Campagnol, I. Stassen, K. Binnemans, D. E. de Vos and J. Fransaer, *J. Mater. Chem. A*, 2015, **3**, 19747–19753.

49 C. Warakulwit, S. Yadnum, C. Boonyuen, C. Wattanakit, A. Karajic, P. Garrigue, N. Mano, D. Bradshaw, J. Limtrakul and A. Kuhn, *CrystEngComm*, 2016, **18**, 5095–5100.

50 F. Caddeo, R. Vogt, D. Weil, W. Sigle, M. E. Toimil-Molares and A. W. Maijenburg, *ACS Appl. Mater. Interfaces*, 2019, **11**, 25378–25387.

51 N. Campagnol, E. R. Souza, D. E. De Vos, K. Binnemans and J. Fransaer, *Chem. Commun.*, 2014, **50**, 12545–12547.

52 J. L. Hauser, M. Tso, K. Fitchmun and S. R. J. Oliver, *Cryst. Growth Des.*, 2019, **19**, 2358–2365.

53 N. Campagnol, T. Van Assche, T. Boudewijns, J. Denayer, K. Binnemans, D. De Vos and J. Fransaer, *J. Mater. Chem. A*, 2013, **1**, 5827.

54 G. G. da Silva, C. S. Silva, R. T. Ribeiro, C. M. Ronconi, B. S. Barros, J. L. Neves and S. A. Júnior, *Synth. Met.*, 2016, **220**, 369–373.

55 M. Li and M. Dincă, *J. Am. Chem. Soc.*, 2011, **133**, 12926–12929.

56 M. Li and M. Dincă, *Chem. Sci.*, 2014, **5**, 107–111.

57 J. Zhao, Y. Wang, J. Zhou, P. Qi, S. Li, K. Zhang, X. Feng, B. Wang and C. Hu, *J. Mater. Chem. A*, 2016, **4**, 7174–7177.

58 M. Li and M. Dincă, *Chem. Mater.*, 2015, **27**, 3203–3206.

59 C. McKinstry, E. J. Cussen, A. J. Fletcher, S. V. Patwardhan and J. Sefcik, *Cryst. Growth Des.*, 2013, **13**, 5481–5486.

60 M. M. Li and M. Dinca, *ACS Appl. Mater. Interfaces*, 2017, **9**, 33528–33532.

61 Q. Zhang, Z. Wu, Y. Lv, Y. Li, Y. Zhao, R. Zhang, Y. Xiao, X. Shi, D. Zhang, R. Hua, J. Yao, J. Guo, R. Huang, Y. Cui, Z. Kang, S. Goswami, L. Robison, K. Song, X. Li, Y. Han, L. Chi, O. K. Farha and G. Lu, *Angew. Chem., Int. Ed.*, 2019, **58**, 1123–1128.

62 X. Kuang, Y. Luo, R. Kuang, Z. Wang, X. Sun, Y. Zhang and Q. Wei, *Carbon*, 2018, **137**, 433–441.

63 Z. Wang, H. Liu, S. Wang, Z. Rao and Y. Yang, *Sens. Actuators, B*, 2015, **220**, 779–787.

64 F. Zhang, Y. Wang, T. Chu, Z. Wang, W. Li and Y. Yang, *Analyst*, 2016, **141**, 4502–4510.

65 H. Liu, H. Wang, T. Chu, M. Yu and Y. Yang, *J. Mater. Chem. C*, 2014, **2**, 8683–8690.

66 L. Besra and M. Liu, *Prog. Mater. Sci.*, 2007, **52**, 1–61.

67 I. Hod, W. Bury, D. M. Karlin, P. Deria, C. W. Kung, M. J. Katz, M. So, B. Klahr, D. Jin, Y. W. Chung, T. W. Odom, O. K. Farha and J. T. Hupp, *Adv. Mater.*, 2014, **26**, 6295–6300.

68 X. Kang, Q. Zhu, X. Sun, J. Hu, J. Zhang, Z. Liu and B. Han, *Chem. Sci.*, 2016, **7**, 266–273.

69 S. H. Huo and X. P. Yan, *Analyst*, 2012, **137**, 3445–3451.

70 Y. S. Seo, N. A. Khan and S. H. Jhung, *Chem. Eng. J.*, 2015, **270**, 22–27.

71 Y. Wang, Y. Zhu, A. Binyam, M. Liu, Y. Wu and F. Li, *Biosens. Bioelectron.*, 2016, **86**, 432–438.

72 H. Zhu, H. Liu, I. Zhitomirsky and S. Zhu, *Mater. Lett.*, 2015, **142**, 19–22.

73 L. E. Kreno, K. Leong, O. K. Farha, M. Allendorf, R. P. Van Duyne and J. T. Hupp, *Chem. Rev.*, 2011, **112**, 1105–1125.
74 W. P. Lustig, S. Mukherjee, N. D. Rudd, A. V. Desai, J. Li and S. K. Ghosh, *Chem. Soc. Rev.*, 2017, **46**, 3242–3285.
75 N. De Acha, C. Elosua, I. Matias and F. J. Arregui, *Sensors*, 2017, **17**, 2826.
76 K. Y. Cheng, J. C. Wang, C. Y. Lin, W. R. Lin, Y. A. Chen, F. J. Tsai, Y. C. Chuang, G. Y. Lin, C. W. Ni, Y. T. Zeng and M. L. Ho, *Dalton Trans.*, 2014, **43**, 6536–6547.
77 W.-J. Li, J. Lü, S.-Y. Gao, Q.-H. Li and R. Cao, *J. Mater. Chem. A*, 2014, **2**, 19473–19478.
78 J. Liu, X. Y. Daphne Ma, Z. Wang, L. Xu, T. Xu, C. He, F. Wang and X. Lu, *ACS Appl. Mater. Interfaces*, 2020, **12**, 7442–7450.
79 F. Zhang, G. Zhang, H. Yao, Y. Wang, T. Chu and Y. Yang, *Microchim. Acta*, 2017, **184**, 1207–1213.
80 Y. Wang, T. Chu, M. Yu, H. Liu and Y. Yang, *RSC Adv.*, 2014, **4**, 58178–58183.
81 J. F. Feng, X. Yang, S. Y. Gao, J. Shi and R. Cao, *Langmuir*, 2017, **33**, 14238–14243.
82 J. F. Feng, S. Y. Gao, T. F. Liu, J. Shi and R. Cao, *ACS Appl. Mater. Interfaces*, 2018, **10**, 6014–6023.
83 J. F. Feng, S. Y. Gao, J. Shi, T. F. Liu and R. Cao, *Inorg. Chem.*, 2018, **57**, 2447–2454.
84 D. Li, X. Cao, Q. Zhang, X. Ren, L. Jiang, D. Li, W. Deng and H. Liu, *J. Mater. Chem. A*, 2019, **7**, 14108–14117.
85 A. C. Power and A. Morri, *Electroanalytical sensor technology*, InTech, Rijeka, 2013, pp. 141–178.
86 R. Michalski and A. Łyko, *Crit. Rev. Anal. Chem.*, 2013, **43**, 100–122.
87 L. Ji, J. Hao, K. Wu and N. Yang, *J. Phys. Chem. C*, 2019, **123**, 2248–2255.
88 P. Hu, X. Zhu, X. Luo, X. Hu and L. Ji, *Mikrochim. Acta*, 2020, **187**, 145.
89 Z. Liu, X. Kuang, X. Sun, Y. Zhang and Q. Wei, *J. Electroanal. Chem.*, 2019, **846**, 113151.
90 Y. Hou, Z. Liu, L. Tong, L. Zhao, X. Kuang, R. Kuang and H. Ju, *Dalton Trans.*, 2020, **49**, 31–34.
91 L. Ji, J. Wang, K. Wu and N. Yang, *Adv. Funct. Mater.*, 2018, **28**, 1706961.
92 L. Wu, Z. Lu and J. Ye, *Biosens. Bioelectron.*, 2019, **135**, 45–49.
93 B. Hoskins and R. Robson, *J. Am. Chem. Soc.*, 1990, **112**, 1546–1554.
94 J. H. Cavka, S. Jakobsen, U. Olsbye, N. Guillou, C. Lamberti, S. Bordiga and K. P. Lillerud, *J. Am. Chem. Soc.*, 2008, **130**, 13850–13851.
95 I. Hod, M. D. Sampson, P. Deria, C. P. Kubiak, O. K. Farha and J. T. Hupp, *ACS Catal.*, 2015, **5**, 6302–6309.
96 L. Wang, Y. Wu, R. Cao, L. Ren, M. Chen, X. Feng, J. Zhou and B. Wang, *ACS Appl. Mater. Interfaces*, 2016, **8**, 16736–16743.
97 B. Zhang, P. Huang, J. Chen, X. Dang, Y. Hu, Y. Ai, D. Zheng and H. Chen, *Appl. Surf. Sci.*, 2020, **504**, 144504.
98 J. Campbell, R. Davies, D. C. Braddock and A. Livingston, *J. Mater. Chem. A*, 2015, **3**, 9668–9674.
99 Y. Mao, J. Li, W. Cao, Y. Ying, L. Sun and X. Peng, *ACS Appl. Mater. Interfaces*, 2014, **6**, 4473–4479.
100 S. Sorribas, P. Gorgojo, C. Téllez, J. Coronas and A. G. Livingston, *J. Am. Chem. Soc.*, 2013, **135**, 15201–15208.
101 H. Guo, G. Zhu, I. J. Hewitt and S. Qiu, *J. Am. Chem. Soc.*, 2009, **131**, 1646–1647.
102 X. Zhang, Y. Li, C. Van Goethem, K. Wan, W. Zhang, J. Luo, I. F. Vankelecom and J. Fransaer, *Matter*, 2019, **1**, 1285–1292.
103 R. Wei, H. Y. Chi, X. Li, D. Lu, Y. Wan, C. W. Yang and Z. Lai, *Adv. Funct. Mater.*, 2019, **30**, 1907089.
104 G. He, M. Dakhchoune, J. Zhao, S. Huang and K. V. Agrawal, *Adv. Funct. Mater.*, 2018, **28**, 1707427.
105 N. Campagnol, R. Romero-Vara, W. Deleu, L. Stappers, K. Binnemans, D. E. De Vos and J. Fransaer, *ChemElectroChem*, 2014, **1**, 1182–1188.
106 M. Naseri, L. Fotouhi, A. Ehsani and S. Dehghanpour, *J. Colloid Interface Sci.*, 2016, **484**, 314–319.
107 S. D. Worrall, H. Mann, A. Rogers, M. A. Bissett, M. P. Attfield and R. A. W. Dryfe, *Electrochim. Acta*, 2016, **197**, 228–240.
108 W. Chaikittisilp, K. Ariga and Y. Yamauchi, *J. Mater. Chem. A*, 2013, **1**, 14–19.
109 J.-K. Sun and Q. Xu, *Energy Environ. Sci.*, 2014, **7**, 2071–2100.
110 X.-W. Liu, T.-J. Sun, J.-L. Hu and S.-D. Wang, *J. Mater. Chem. A*, 2016, **4**, 3584–3616.
111 K. Shen, X. Chen, J. Chen and Y. Li, *ACS Catal.*, 2016, **6**, 5887–5903.
112 Z. Song, N. Cheng, A. Lushington and X. Sun, *Catalysts*, 2016, **6**, 116.
113 X. Cao, C. Tan, M. Sindoro and H. Zhang, *Chem. Soc. Rev.*, 2017, **46**, 2660–2677.
114 H. B. Wu and X. W. D. Lou, *Sci. Adv.*, 2017, **3**, eaap9252.
115 H. Zhang, J. Nai, L. Yu and X. W. Lou, *Joule*, 2017, **1**, 77–107.
116 X. Zhang, J. Luo, P. Tang, X. Ye, X. Peng, H. Tang, S.-G. Sun and J. Fransaer, *Nano Energy*, 2017, **31**, 311–321.
117 X. Zhang, J. Luo, P. Tang, J. R. Morante, J. Arbiol, C. Xu, Q. Li and J. Fransaer, *Sens. Actuators, B*, 2018, **254**, 272–281.
118 J. Linnemann, L. Taudien, M. Klose and L. Giebeler, *J. Mater. Chem. A*, 2017, **5**, 18420–18428.
119 G. Zhao, X. Sun, L. Zhang, X. Chen, Y. Mao and K. Sun, *J. Power Sources*, 2018, **389**, 8–12.
120 X. Kuang, R. Kuang, Y. Dong, Z. Wang, X. Sun, Y. Zhang and Q. Wei, *Inorg. Chem.*, 2019, **58**, 3683–3689.
121 S. Dang, Q.-L. Zhu and Q. Xu, *Nat. Rev. Mater.*, 2017, **3**, 17075.
122 M. J. Van Vleet, T. Weng, X. Li and J. R. Schmidt, *Chem. Rev.*, 2018, **118**, 3681–3721.
123 S. Yuan, L. Feng, K. Wang, J. Pang, M. Bosch, C. Lollar, Y. Sun, J. Qin, X. Yang, P. Zhang, Q. Wang, L. Zou, Y. Zhang, L. Zhang, Y. Fang, J. Li and H. C. Zhou, *Adv. Mater.*, 2018, 1704303.
124 M. Zhao, Y. Huang, Y. Peng, Z. Huang, Q. Ma and H. Zhang, *Chem. Soc. Rev.*, 2018, **47**, 6267–6295.